ARMY RESEARCH LABORATORY

Adding Weather to Wargames

by
Sean G. O'Brien and Richard C. Shirkey

ARL-TR-4005 **January 2007**

NOTICES

Disclaimers

The findings in this report are not to be construed as an official Department of the Army position unless so designated by other authorized documents.

Citation of manufacturer's or trade names does not constitute an official endorsement or approval of the use thereof.

Destroy this report when it is no longer needed. Do not return it to the originator.

Army Research Laboratory
White Sands Missile Range, NM 88008-5501

ARL-TR-4005 **January 2007**

Adding Weather to Wargames

Sean G. O'Brien and Richard C. Shirkey
Computational Information Sciences Directorate

REPORT DOCUMENTATION PAGE	*Form Approved OMB No. 0704-0188*

1. REPORT DATE *(DD-MM-YYYY)*	**2. REPORT TYPE**	**3. DATES COVERED (From - To)**
January 2007	Final	2003-2006

4. TITLE AND SUBTITLE Adding Weather to Wargames	**5a. CONTRACT NUMBER** NA
	5b. GRANT NUMBER
	5c. PROGRAM ELEMENT NUMBER
6. AUTHOR(S) Sean G. O'Brien and Richard C. Shirkey	**5d. PROJECT NUMBER**
	5e. TASK NUMBER
	5f. WORK UNIT NUMBER
7. PERFORMING ORGANIZATION NAME(S) AND ADDRESS(ES) U.S. Army Research Laboratory Computational and Information Sciences Directorate Battlefield Environment Division (ATTN: AMSRD-ARL-CI-EE) White Sands Missile Range, NM 88002-5501	**8. PERFORMING ORGANIZATION REPORT NUMBER** ARL-TR-4005
9. SPONSORING/MONITORING AGENCY NAME(S) AND ADDRESS(ES) U.S. Army Research Laboratory 2800 Powder Mill Road Adelphi, MD 20783-1145	**10. SPONSOR/MONITOR'S ACRONYM(S)** **11. SPONSOR/MONITOR'S REPORT NUMBER(S)**

12. DISTRIBUTION/AVAILABILITY STATEMENT
Approved for public release; distribution is unlimited.

13. SUPPLEMENTARY NOTES

14. ABSTRACT
Employing the capability of the Target Acquisition Weapons Software (TAWS) tactical decision aid, and the rules embodied in the Integrated Weather Effects Decision Aid (IWEDA) we developed techniques that allowed significant improvement in weather effects and impacts for wargames. TAWS was run for numerous and varied weather conditions; the resultant database was subsequently used to construct third-order polynomial curves to represent infrared sensors acquiring targets under those weather conditions. IWEDA rules were used in determination of go/no-go weather situations for platforms or systems. We found that the wargame realism was increased without impacting the run time. While these techniques are applicable to wargames in general, we tested them by incorporation into the Advanced Warfighting Simulation (AWARS) model. AWARS was modified to incorporate weather impacts upon sensor operation and platform mobility. These modifications included revision of the direct-fire sensor detection algorithm to reflect variations of the maximum number of resolution cycles over the direct fire target with meteorological visibility, time of day, sky cover, target state, and haze aerosol type. The speed of these computations was an important consideration, so the parametric fit technique was selected after a favorable comparison with table look-up methods. Weather effects upon combatant platform mobility were modeled by implementation of IWEDA rules classes for both helicopters and fixed-wing aircraft platforms. The impacts of these modifications in both the presence and absence of adverse weather conditions were tested and are summarized.

15. SUBJECT TERMS
Wargames, weather, sensors, rules, parametric curve fits, target acquisition

16. SECURITY CLASSIFICATION OF:			**17. LIMITATION OF ABSTRACT**	**18. NUMBER OF PAGES**	**19a. NAME OF RESPONSIBLE PERSON**
a. REPORT	**b. ABSTRACT**	**c. THIS PAGE**			Sean G. O'Brien
U	U	U	SAR	85	**19b. TELEPHONE NUMBER** (*Include area code*) (505) 678-1570

Standard Form 298 (Rev. 8/98)
Prescribed by ANSI Std. Z39.18

Contents

List of Figures

List of Tables

Acknowledgments

We would like to thank Terry Gach and Steven Glasgow, TRADOC Analysis Center (TRAC)-Ft. Leavenworth, for many interesting discussions and aiding in obtaining Advanced Warfare Simulation (AWARS). In addition they were instrumental in setting up the scenario and interpretation of the results.

Executive Summary

We have developed techniques to improve wargame realism without impacting their run time by using the Tri-Service Target Acquisition Weapons Software (TAWS) tactical decision aid and the rules embodied in the Integrated Weather Effects Decision Aid (IWEDA). This was accomplished by constructing parametric curves representing the probability of detection for sensor target acquisition under varied weather conditions, in conjunction with system "critical values" for quick determination of go/no-go weather situations for platforms or systems. For initial engagement, critical weather values, or rules, initially developed for the Army Research Laboratory/Battlefield Environment Division's (ARL/BED) IWEDA, were used for quick assessments. For atmospheric effects on sensor systems, we employed TAWS to develop quick running polynomial curves for various weather conditions coupled with various sensors and target types.

To implement and verify our techniques, we made weather modifications to the Advanced Warfare Simulation (AWARS), developed by TRAC-Ft. Leavenworth. The AWARS model is designed to simulate attrition effects at a finer scale than many other models at a unit and platform level of detail. The AWARS designers have also incorporated a comprehensive weather event class library to describe the evolution of weather conditions during the course of the AWARS wargame scenario. This library of classes can describe both global (scenario-wide) conditions (the default) and conditions that are limited to specific sub-regions of the scenario terrain. This latter scoping capability is useful for description of localized weather effects such as rain or snow squalls, lofted dust clouds, or fog banks that appear due to terrain effects or natural inhomogeneities in the weather.

We first modified the direct fire (DF) portion of the AWARS model to reflect impacts that time of day, cloud cover, haze aerosol type, target operational state, and meteorological visibility have upon the maximum number of resolvable angular spatial cycles that can be seen over the span of the target by a particular sensor. The sensors that we used for this effort were from the TAWS long-wave infrared (LWIR) set. These sensors are carried by Service ground and air platforms, so that weather impacts to their performance would be widely felt. This was borne out in tests that we performed comparing unit attrition rates under various visibility conditions.

As a precursor to adding DF weather modifications to the AWARS code, we exercised the TAWS model over a widely-spanned, but coarsely-gridded parameter space. We considered tank and armored personnel carrier (APC) targets in both exercised (hot) and inactive (cold) operational states, with the sensor pivoted about the target at the four cardinal compass directions. Morning (0900 local time) and afternoon (1500 local time)

times of day were considered, as well as cloudless and overcast sky cover. Two aerosols, advection fog and rural background, were used at four visibilities: 0.1, 1, 10, and 100 kilometers.

The sensor curves were normalized with respect to maximum detection range for the given sensor, and were then averaged (or "aggregated") over target type, sensor type, sensor orientation (with respect to the target), and meteorological conditions (sky cover, aerosol type, and visibility), time of day and location. The aggregation, which is an option in the codes, was done to examine the possibility of ignoring certain orientations, times of day, weather conditions, etc. The normalized response data were then fit with third degree polynomials in log visibility, with the resulting fit coefficients recorded as data members of a new class in the AWARS code. The maximum detection range for each sensor under the same meteorological conditions was also encapsulated as a data member in this new class. Thus, when a given set of atmospheric conditions are encountered during the course of an AWARS scenario, the normalized sensor detection range curve is constructed, that range is rescaled by the particular sensor's maximum detection range under those conditions, and the result is then used to compute a maximum number of resolvable cycles over the target for the target detection task. The resolvable cycles criterion is subsequently used in a target detection model to determine the time required by the sensing platform to acquire its target and to begin the attrition process.

The next modification phase involved application of the IWEDA meteorological impacts rules set to determine the ability of airborne platforms to participate in the AWARS combat scenario as it evolves. The first class of platforms that received this revision was the helicopter unit (in both its attack and reconnaissance forms). A new class was created to handle both the generic IWEDA rule and the specific application of the IWEDA rule to the helicopter platform. The mobility methods were then modified and used by helicopter platforms so that the weather-induced grounding or mission abort events could be effectively simulated. We also performed corresponding modifications for fixed wing aircraft platforms using the same base IWEDA rule class and a new class that was tailored to interface with a fixed wing platform entity. Tests of these modifications were performed internally.

We further examined and summarized the impacts that application of IWEDA rule restrictions and TAWS parametric curves would have upon unit attrition levels and attrition timing for a small AWARS scenario. Although the expected results were obtained without any significant increase in run time, they clearly demonstrated the importance of weather effects upon combat unit attrition rates. Asymmetries in the sensor technologies and platform mobility employed by opposing forces should tend to magnify weather-induced changes in attrition exchange rates. These trends may be explored by application of our modifications.

While our techniques were applied to AWARS, they are applicable to a wide range of wargames. Also, since the IWEDA rule set and the TAWS tactical decision aid both contain data relevant to all Services, our techniques can be applied to Army, Navy, and Air Force wargames.

INTENTIONALLY LEFT BLANK.

1. Overview

Army operations research (OR) relies heavily on wargame simulations, which range from detailed one-on-one models to aggregated models. These provide essential information for the mission planner and/or analyst, both of whom are striving for emulation of real-world events to improve Army effectiveness. To quote from the introduction of Bracken, et al., Wargame Modeling (*1*),

> "The spectrum of military OR spans from detailed, high-resolution microscopic analysis to highly aggregate macroscopic analysis. At the detailed end, specific attributes of certain weapon systems are assessed using statistics and probability techniques, which are incorporated in simulations or analytic models. Next on that spectrum are operational problems relating to force structure, combat development and tactics. These are often analyzed using combat models… which are sets of deterministic or stochastic differential or difference equations representing attrition in combat."
>
> "At the low-resolution, macroscopic end of the spectrum of military OR analyses are theater problems and strategic issues. These are usually treated by highly aggregate combat models and game-theoretic methods."

Aggregate wargames are typically analytical simulations of Joint Service campaign-level warfare for use by theater-level combat command staffs, the Joint Staff, and the various Services. They support courses of action analyses, force structure capability assessments, force structure tradeoffs, cost and operational effectiveness analyses, and joint warfare capability assessments. Table 1 lists the most common wargame simulations the Army uses (*2*, *3*); for completeness some of the Joint wargame models are also listed (*4*, *5*).

Table 1. Some common Army and Joint Wargames.

Army			
Advanced Warfighting Simulation (AWARS)	Combined Arms Support Task Force Evaluation Model (CASTFOREM)	Combined Arms Analysis Tool for the XXIst Century (COMBAT XXI)	Corps Battle Simulation (CBS)
Concepts Evaluation Model (CEM)	JANUS	One Semi-automated Forces (OneSAF)	Vector in Commander (VIC)
Warfighter's Simulation (WARSIM)			
Joint			
Joint Conflict and Tactical Simulation (JCATS)	Joint Simulation System (JSIMS)	Joint Warfare System (JWARS)	Tactical Warfare Model (TACWAR)

The very nature of wargames requires that they run faster than real time - ratios of 1000:1 are not atypical. As one might expect, setup times are also lengthy and require input from varied sources. However, meaningful simulation results depend significantly upon the accurate characterization of battlefield weather and its impact upon combat and surveillance sensors. As computing and network data transmission speeds have improved, the design emphasis on many of the current constructive models has tended toward more detailed structural and functional descriptions of combat units and terrain, rather than a more complete description of sensor interactions with the atmospheric environment. This situation is understandable, because the foundations of Army wargames are the individual combat units, the terrain that they fight upon, and the application of tactical doctrine that determines the outcome of their interactions. Detailed descriptions for contemporary vehicles, weapon systems, terrain, and tactics evolve relatively slowly and allow for timely and concise implementation in constructive simulations. Sensor technology evolves more rapidly and the comprehensive characterization of atmospheric effects upon sensors demands considerable computer resources. Consequently, the priority assigned to implementing treatments of these devices and phenomena in wargames has historically not been the highest possible.

The Army Research Laboratory, Battlefield Environment Division (ARL/BED) has developed a methodology for realistically adding weather effects and impacts to wargames. For initial engagement, critical weather values, or rules, initially developed

for ARL's Integrated Weather Effects Decision Aid (IWEDA), are used for quick go/no-go assessments. For atmospheric effects on sensor systems, we have employed the Tri-Service Target Acquisition Weapons Software (TAWS) to develop quick running parametric curves for various weather conditions coupled with various target types.

To implement and verify our techniques, we have made weather modifications to the Army Warfare Simulation (AWARS), developed at TRAC-Ft. Leavenworth. The AWARS model is designed to simulate attrition effects at a finer scale than many other models at a unit and platform level of detail. The AWARS designers have also incorporated a comprehensive weather event class library to describe the evolution of weather conditions during the course of the AWARS wargame scenario. This library of classes can describe both global (scenario-wide) conditions and conditions that are limited to specific sub-regions of the scenario terrain. This latter scoping capability is useful for description of localized weather effects such as rain or snow squalls, lofted dust clouds, or fog banks that appear due to terrain effects or natural inhomogeneities in the weather.

2. Introduction

While computer speed has increased dramatically over the past years, it still is not fast enough to account for all wargame processes, particularly weather and weather effects. ARL/BED is developing new techniques to address this problem. First, we are using weather "critical values" that provide qualitative weather impacts for platforms, weapon systems, and operations, including soldier performance. These critical weather values, or rules, currently used in the IWEDA (*6*) transform raw weather data into weather impacts. IWEDA's collection of rules, with associated critical weather values, aids the commander in selecting appropriate operations, platforms, systems, sub-systems, components, or personnel under given or forecast weather conditions. Each system (Army, Air Force, Navy, and threat) has its list of relevant rules, which include red-amber-green (unfavorable-marginal-favorable) critical value weather thresholds for one or a combination of the environmental parameters that affect the system. An example of such a system "red" rule might be "surface winds greater than 30 knots preclude helicopter takeoff or landing." An example of an "amber" rule for helicopters might be "surface wind speed greater than 27 knots may impact aircraft hover." Such rules, when implemented in a wargame, can be assigned a "success" probability that would allow a percentage of helicopters to take off or hover; by assigning a success rate less than one, the subsequent play of the wargame would be impacted. The rules may also be used in go/no-go situations such as heavy rain, thick fog, heavy icing aloft, etc. This latter type of implementation is easily accomplished and the impacts are clearly delineated. Thus,

these types of rules can provide relevant and quick information. However, not all such rules do so; in the case of sensors the rules are not so clear cut. For example, a "red" rule for sensors might be "if visibility is less than 1 km, target detection is not possible" and a "yellow" rule might be "if visibility is greater than 1 km, but less than 5 km, target acquisition is impaired." Obviously rules related to sensors provide only general guidance, useful for sensor selection but not for target acquisition where the ability of a sensor to acquire a target diminishes as the weather degrades. In addition, the type of sensor, its operational wavelength band and the background against which a particular target is being viewed, are all additional factors that must be considered in target acquisition. The Tri-Service TAWS (*6*) has been designed to provide detection, recognition, identification, and lock-on range predictions for selected sensors and targets using physics-based models in conjunction with the Night Vision and Electronic Sensors Directorate's (NVESD) Acquire (*7*) algorithm, using input or forecast weather conditions. While TAWS runs relatively rapidly, it still does not approach the high execution speeds required to assess weather impacts on the many individual sensors that are present in simulations. Thus, while TAWS has the capability to calculate such effects for varied sensors, targets, and weather conditions, setup and run time preclude its direct inclusion into wargames. Therefore, our second, complementary technique, for dealing with weather effects on sensors uses TAWS results to construct parametric curves yielding predictions of sensor performance that do execute with the requisite speed.

Remaining sections in this document explain the current and modified weather structure in AWARS, and the construction, testing and implementation of algorithms that determine weather effects and impacts on Army systems.

3. AWARS Weather

3.1 Current AWARS Weather Structure

Weather has the ability to affect nearly all the functional areas within the AWARS simulation. To this end it is important that AWARS represent weather that is appropriate for this level of simulation, changes over time and is easy for developers to integrate.

Weather needs to be accessible to most entities in the simulation. Terrain itself is actually affected by weather in some cases, but direct weather-terrain interactions are not considered in this report. To access weather information in AWARS requires that some capability exist to return weather information based on a given location. Desired weather conditions should include (but are not limited to) percent cloud cover, humidity, and temperature and wind speed for various altitudes.

In the version of AWARS used here, a structure already exists that divides the battlefield into a grid system within the terrain packages. The application code interfaces to the terrain representation through terrain objects and retrieves information about relief and vegetation for these objects.

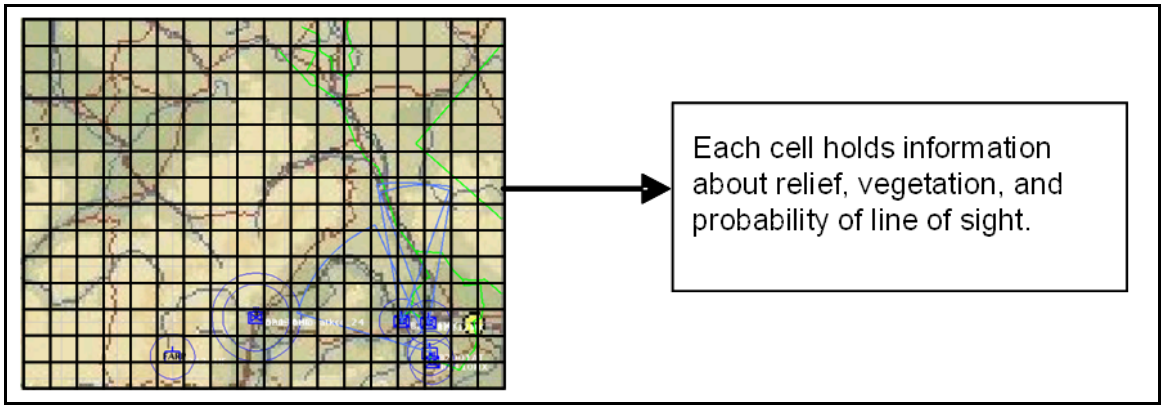

Figure 1. AWARS terrain cell objects have linkages to other external objects in the scenario.

The terrain implementation in AWARS also has connectivity to a weather class hierarchy. This was designed to encapsulate weather events that are scripted in a file that is loaded at the beginning of an AWARS scenario run. Figure 2 illustrates how this scripted weather mechanism is implemented in the AWARS executive control flow.

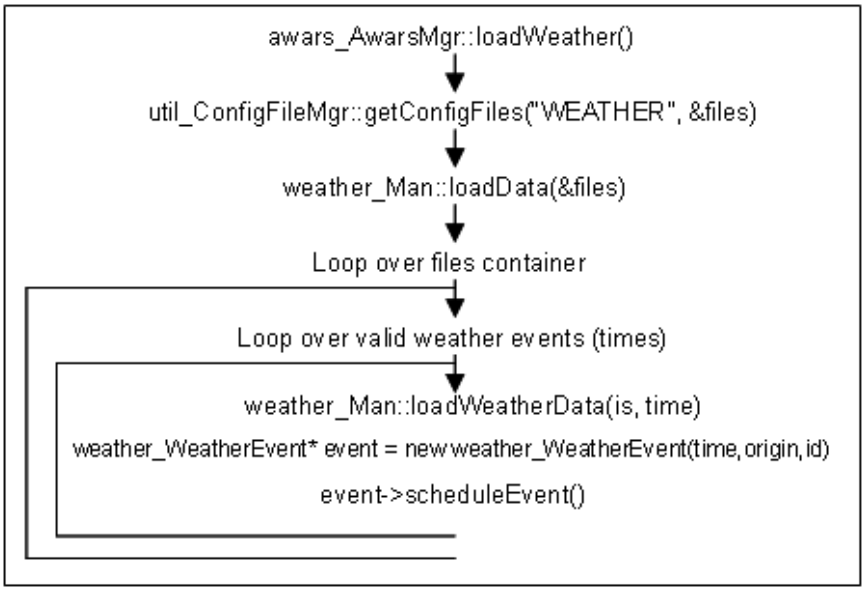

Figure 2. AWARS control flow for loading of scripted weather events.

As can be seen in figure 2, several additional classes are used in the weather event setup. The main AWARS executive class, awars_AwarsMgr, begins the process when it invokes its loadWeather() method. The getConfigFiles() method of a util_ConfigFileMgr

object retrieves a pointer to a list of weather event files. This list is then sequentially cycled to extract and schedule weather events. The weather_Man and weather_Event classes manage the access to the basic descriptor class for weather, the weather_Weather class, which is shown in a class diagram in figure 3. This figure lists the public ("+" prefix) and private ("-" prefix) data members and methods for this class.

Figure 3. Member functions and data members of the AWARS weather_Weather class.

The weather_Weather class in turn accesses weather parameter classes to allow referencing objects fine-grained control over weather information that they can request.

Figure 4 depicts the data members and methods for some of these additional parameter classes.

Note that the default geographic span for a weather event is the entire terrain map. If it is desired that more localized events be specified (for example, snow squalls or thunderstorms), additional geometric shape classes are provided. Additional meteorological parameter and shape classes can be added as needed.

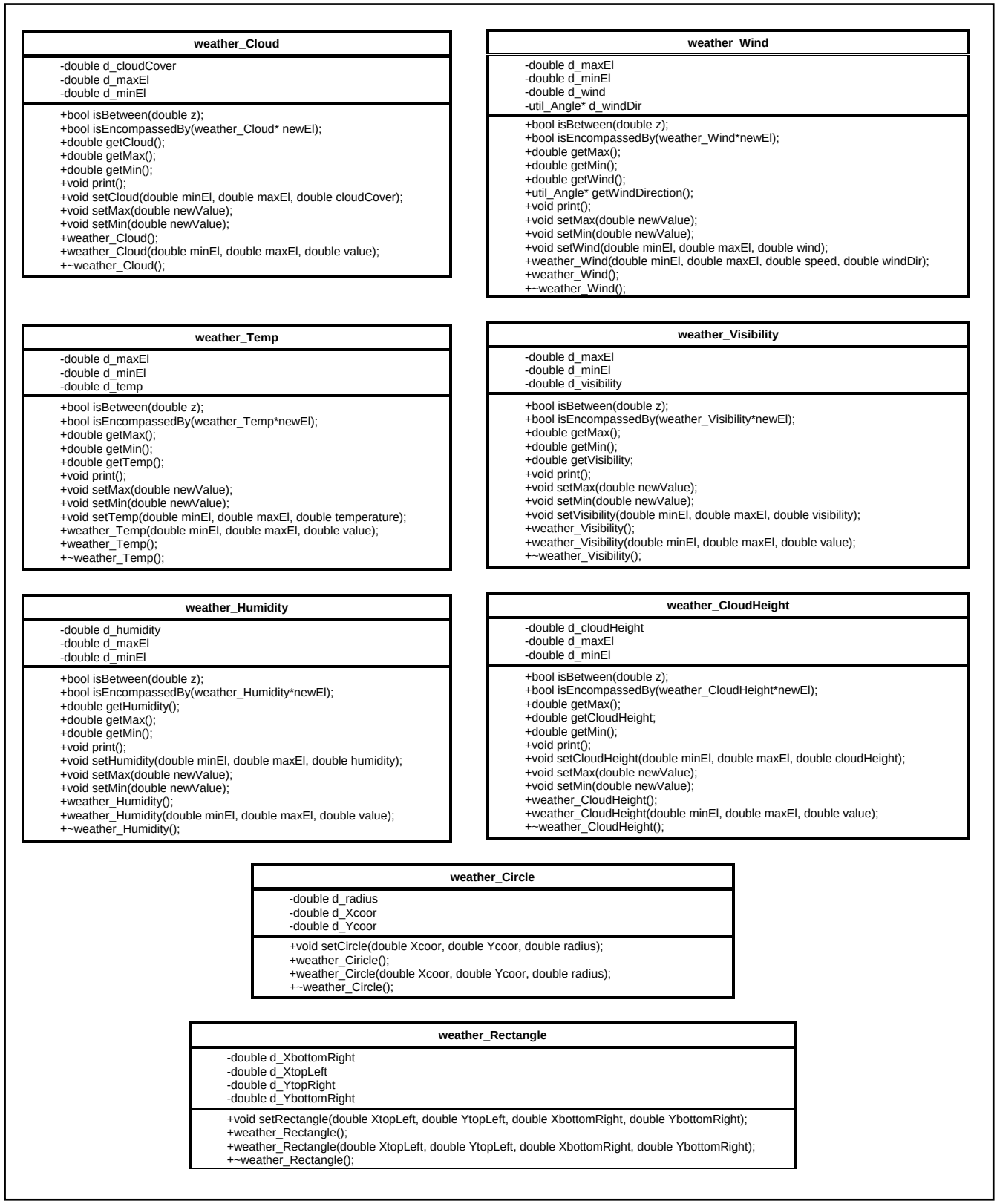

Figure 4. Weather parameter classes used in AWARS by the weather_Weather class.

3.2 Modification of AWARS Weather Structure

We incorporated weather effects and impacts algorithms into AWARS in such a fashion that they are represented without impacting AWARS run time. Specifically, we modified the Intelligence Surveillance and Reconnaissance (ISR) acquisition algorithms and Command and Control (C2) processes. The approach used here was to use TAWS to construct parametric curves for ISR allowing for a more realistic representation of target acquisition under varied weather conditions. Second, we incorporated IWEDA rules into AWARS for C2 allowing for a quick go/no-go analysis. Both approaches have little or no impact on AWARS run time.

To accomplish this, we divided the effort into several distinct execution phases that had very little interdependence either in theory or in the implemented code. This permitted isolation of the modified code so that the results of each phase could be separately tested and revised. We first added weather effects to the direct fire (DF) portion of the code where air and ground units exchange fire and attrition is most directly affected by the weather. Next, we implemented IWEDA rules for weather impacts upon the mobility of helicopter (helo) platforms. We then extended this mobility impacts approach to cover fixed-wing aircraft (FWA) platforms after tests of the IWEDA rule interface produced demonstrable effects. Figure 5 depicts the library directories and code files that have been affected by these changes.

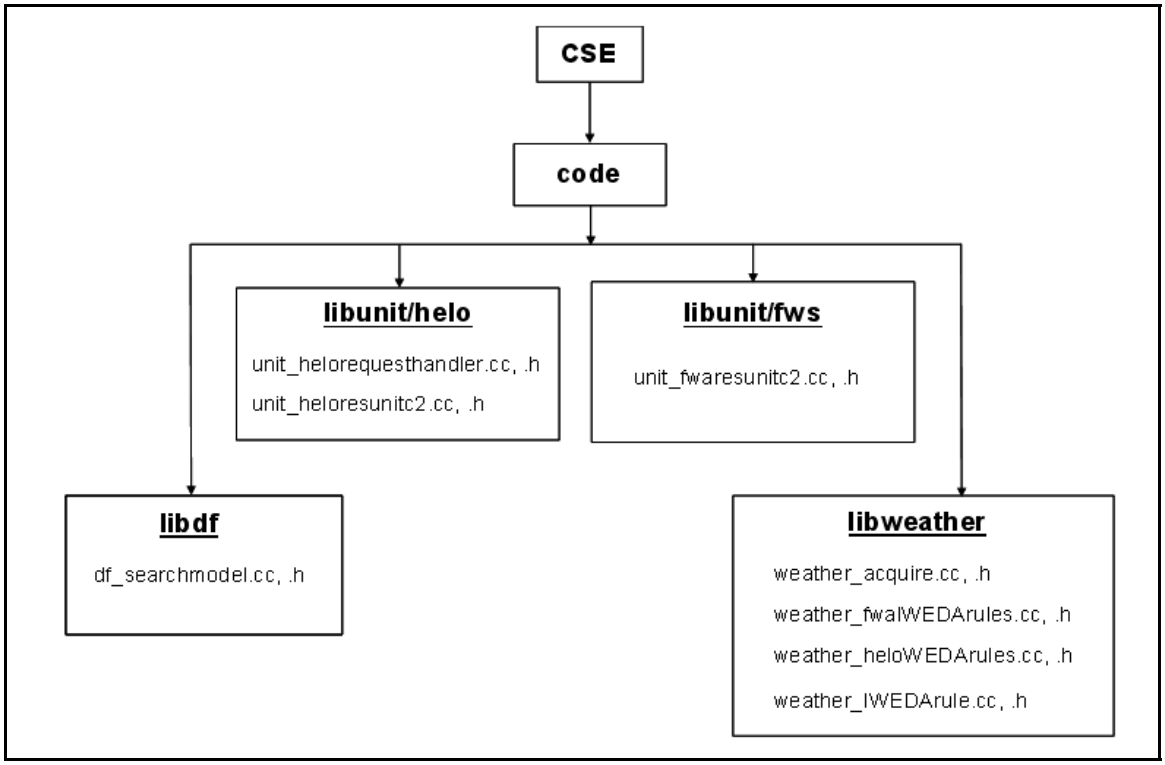

Figure 5. AWARS library directories and code files affected by weather effects implementation.

4. Development of the Parametric Curves

4.1 Parametric Curves vs. Tabular Lookup

Before we implemented algorithms containing parametric curves, it was necessary to determine if that approach would be faster than the current tabular lookup in AWARS. Differences in AWARS run time for these two techniques was inferred by examining run time determined using the parametric curves with the time required when accessing acquisition ranges from tables.

This was done using various compilers and, in 2003, state-of-the art computer systems. We used Silicon Graphics® (SGI®) machines running under the IRIX® 6.5 operating system with a CPU speed of 175 megahertz (MHz) and the native GNU FORTRAN77 and GNU C compilers. In addition we used PC machines running under Red Hat® 8.0 with Intel® CPU speeds of 400 and 930 MHz and the GNU FORTRAN77, Lahey™ FORTRAN90, GNU C and Microsoft Visual C++® compilers. Since, in a wargame, target acquisition information may be called for a large number of times, we performed our tests with 10^7 operations. As may be seen in figures 6 and 7, the parametric curves provided a significant improvement over accessing the tables.

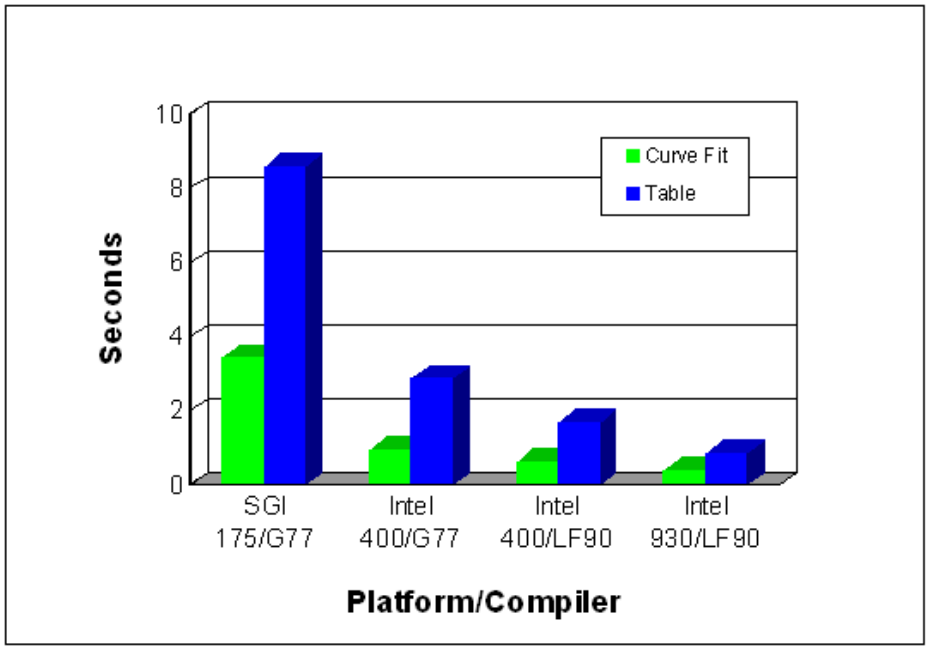

Figure 6. FORTRAN run time comparison: parametric curves vs. tabular lookup for 10^7 operations.

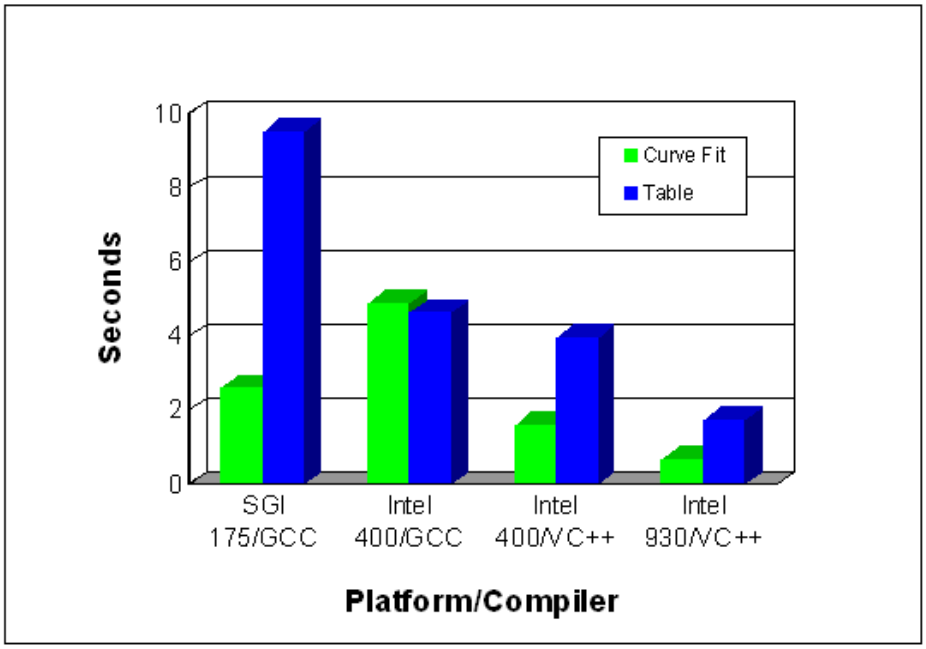

Figure 7. C run time comparison: parametric curves vs. tabular lookup for 10^7 operations.

4.2 Parametric Curve Construction

TAWS version 2.2 was used to determine detection ranges as a function of weather using infrared (IR) sensors coupled with various targets. A series of codes, written in FORTRAN90, were constructed to read the TAWS output file (met.dat). This file was examined for errors–sensors that had only one field of view (FOV) or excessively large ranges were excluded. A second program optionally averaged over the various weather parameters (see table 2), primarily as a function of sensor FOV, time of day (TOD) and aerosol type. Once these averages were available, the detection ranges for the various combinations were normalized to an average maximum detection range and subsequently fit to a third-order polynomial (*8*). While we were interested in examining sensor averages, the codes were also generated to examine a specific sensor's response to varying meteorological conditions.

At the time of the initial study, TAWS contained 26 different sensors, many of which had narrow FOVs (NFOV) and wide FOVs (WFOV), 7 army-type vehicular targets with 4 (N, S, E, W) orientations and 3 operational modes (off, idled, exercised), 23 stationary targets, 7 surface weather types, 6 cloud types, and other sundry quantities. Since there are an unlimited number of conditions (weather, sensor, target, TOD, location) that could occur on the battlefield, we initially determined weather impact on sensors by aggregating many of these conditions. However, aggregating this number of possibilities would have been next to impossible and would have provided meaningless results. Thus, we restricted our parameter space to cover all 26 sensors, 2 targets with all orientations

and 2 operational states, 3 seasons, 2 locations, 2 TOD, 4 visibilities, 2 aerosol types, and 1 cloud type. These parameters are presented in table 2.

Table 2. Parameter space used for determination of the DF curves.

Sensors ▪ FOV ▪ platform	26 IR ▪ narrow and wide ▪ helicopter @ 300’ altitude
Targets ▪ state ▪ orientation	T-80, APC ▪ off & exercised ▪ N, S, E, W
Meteorology ▪ visibility ▪ aerosols ▪ cloud cover	 ▪ 0.1, 1.0, 10, 100 km ▪ rural, fog (moderate radiation) ▪ clear, overcast
Locale ▪ longitude ▪ latitude ▪ background	 ▪ 0° ▪ 0°, 30° N ▪ Desert sand
Season ▪ 0° ▪ 0°, 30° N	 ▪ equinox & winter solstice ▪ summer & winter solstices
TOD	0900 & 1500

TAWS was run for all 26,624 possible combinations listed in table 2 and the results concatenated into a database. Using this database, we could aggregate the results over the quantities in table 2, e.g.:

- location / season,
- aerosol type,
- cloud cover / clear air,
- FOV,
- Line of Sight (LOS) azimuth,
- sensor,
- target type,
- target operation state.

However, given the large number of possible combinations that could be made using the database, we averaged over 116 arbitrary chosen combinations, and determined detection range primarily as a function of:

- visibility,
- aerosol type, and
- FOV.

These results were then normalized using the average maximum detection range as determined by the 100 km visibilities. This provided us with four normalized detection ranges as a function of the four visibilities which we then curve fit to a third-order polynomial.

4.2.1 Examples

An example of a resultant curve for the two aerosol types (fog and rural) and two atmospheric conditions (clear and overcast) at 0900 is shown in figure 8; the same conditions, but at 1500, are shown in figure 9.

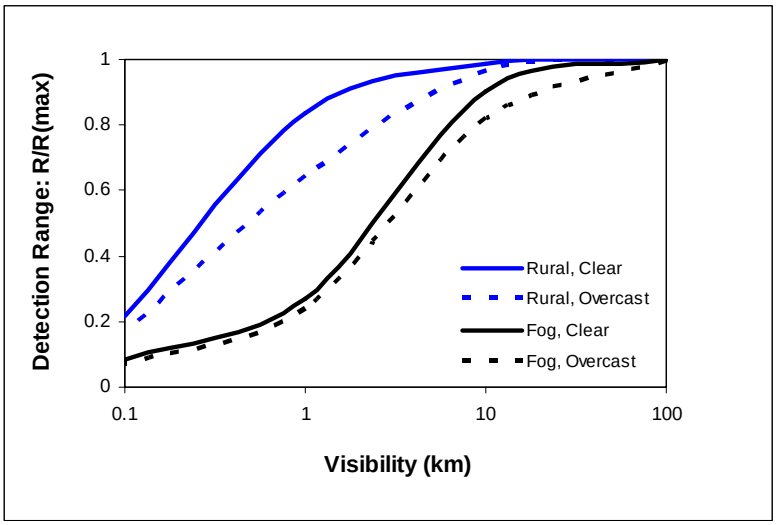

Figure 8. Normalized detection range as a function of aerosol type and visibility for an average sensor and vehicle type at 0900.

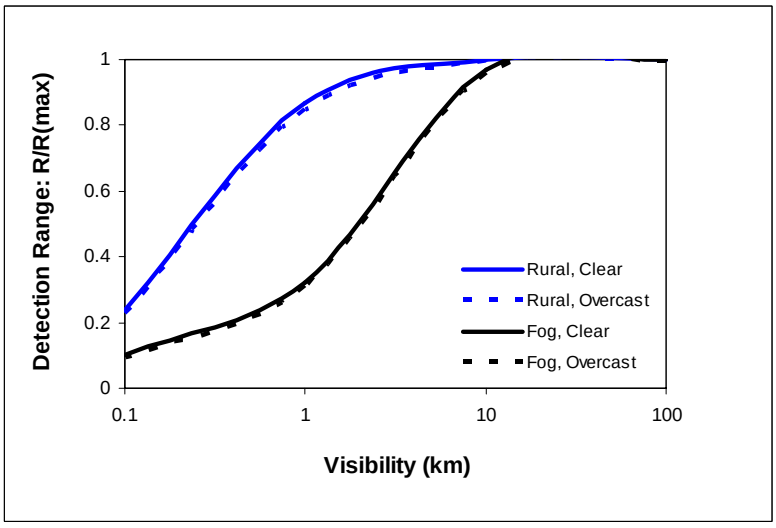

Figure 9. Normalized detection range as a function of aerosol type and visibility for an average sensor and vehicle type at 1500.

Figures 8 and 9 show a rather interesting result: regardless of TOD, detection range is not heavily dependent upon cloud cover but is dependent upon aerosol type. The explanation for this is fundamental to the aerosol extinction; the rural extinction coefficient is 0.78 km^{-1} and the fog extinction coefficient is 0.87 km^{-1} or 12% higher per kilometer, leading to lower detection ranges in the fog aerosol. Inter-comparison of figures 8 and 9 shows the effects of TOD where we can see that, under clear conditions, the vehicles heat up more rapidly when compared to the desert background. We also note that this does not occur anywhere to the same degree when the conditions are overcast and the upwelling radiation is trapped, leading to more uniform temperature conditions. Appendices B (fog aerosol) and C (rural aerosol) contain the third-order polynomial coefficients for the 116 combinations for both NFOV and WFOV, and a sub-set of over 120 curves concatenated into 30 graphs. Inspection of these graphs provides insight into whether or not this technique is providing correct results. For example, the graphs show that it is always more difficult to detect targets in the afternoon, as determined by the 1500 curves, than it is in the morning (the 0900 curves); this is due to the increased ground temperature in the afternoon making the ΔT between target and background smaller. They also show that it is easier to detect an exercised tank, under all conditions, than it is an off tank, although the difference in detection range is less in the summer than in the winter. In the winter the disparities between morning and afternoon detection ranges are greater due to the relatively larger surface temperature ranges. Although these differences in detection ranges can easily be explained due to differing surface and tank temperatures and their underlying albedos, there are some apparent anomalies when examining this premise as a function of azimuth angle. For example, in all of the figures with the tank exercised, the northerly viewing direction has the highest detection range. The reason for this becomes apparent when viewing figure 10, which shows the scenario geometry and additionally depicts the tank's exhaust. The target heading was always north, thus when viewing in a northerly direction, the tank exhaust provides an overall hotter temperature, leading to longer detection ranges. These and many other frequently obvious effects can be determined from the graphs, thus validating our technique.

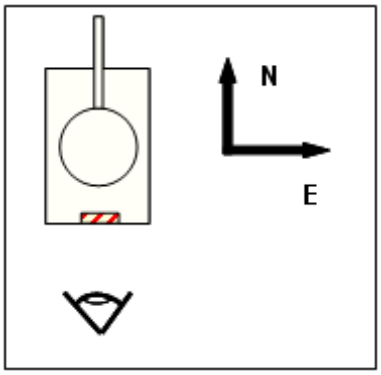

Figure 10. Scenario is looking north, with the exhaust at the rear of the tank.

Many of the curves exhibit an overshoot at visibilities greater than 10 km. This is clearly due to the limited number of points used for construction of the polynomial curve: TAWS' calculations with additional visibilities would correct this situation. Also, many of the figures in appendices B and C require extreme magnification to differentiate the various curves, since a slight variation in atmospheric conditions may only produce a

slight difference in detection range, and some combinations may produce detection ranges that are nearly identical to other, different, combinations.

4.3 Implementation for DF

The TAWS results described in the preceding were encapsulated into a new class called weatherAcquire that resides in the AWARS libweather subdirectory and operates in conjunction with the df_SearchModel class in the libdf subdirectory. We examined the df_SearchModel class to identify an appropriate algorithmic method and point in the code where the DF behavior of both ground and airborne entities could be modified by local weather conditions. The DF target search algorithm used in AWARS is essentially the NVESD Acquire model, which applies a resolvable angular cycles-over-target criterion to determine the probability that the target has been detected at a given range and set of scenario conditions. This algorithm is implemented in the df_SearchModel::acquire() method, as depicted in figure 11.

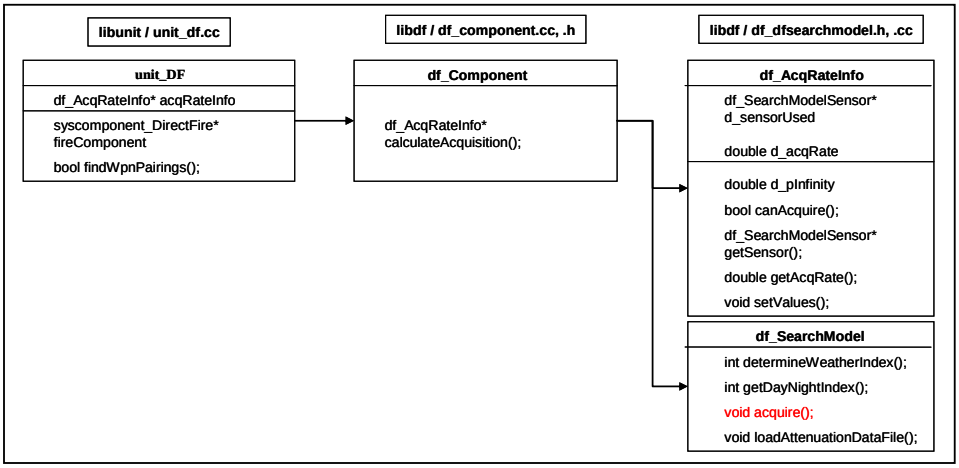

Figure 11. Dependency chain used to determine DF weather modification placement.

The Acquire algorithm approximates the asymptotic (infinite time) probability of detection P_∞ as a function of the maximum number of spatial resolution cycles N over the target as a function of the form

$$P_\infty = \frac{\left[N/\left(N_{50}\right)_D\right]^E}{1+\left[N/\left(N_{50}\right)_D\right]^E}, \tag{1}$$

where

$$E = 2.7 + 0.7\left[N/\left(N_{50}\right)_D\right], \tag{2}$$

and $(N_{50})_D$ is the number of cycles required for 50% detection probability by a representative ensemble of observers. The $(N_{50})_D$ value is dependent upon the level of

background clutter in which the target is embedded, ranging from 0.5 cycles in low clutter to 2 cycles in high clutter environments. The value that we used in our weather effects modification is 0.75 cycle, which is midway between the low clutter (0.5 cycle) and moderate clutter (1 cycle) values. The determination of the quantity *N*, the maximum number of resolvable cycles across the target, is the central point at which we apply DF weather modifications. The target critical dimension H_{targ}, target range *R*, and maximum resolvable spatial frequency f_x for the given sensor at the apparent target ΔT (in units of cycles per radian) are related to *N* by the relation (*9*)

$$N = f_x \frac{H_{targ}}{R}. \tag{3}$$

The maximum resolvable spatial frequency f_x for a given maximum detection range R_D is also given by the expression

$$f_x = \frac{\left(N_{50}\right)_D}{H_{targ} \big/ R_D}, \tag{4}$$

where R_D is a function of sensor type, meteorological visibility *V*, TOD, cloud cover, target state, and haze aerosol type. We determine R_D through application of the TAWS parametric curves developed above:

$$R_D = R_{D100}\, \Re(V), \tag{5}$$

where R_{D100} is the TAWS unlimited visibility detection range (considered to be 100 km visibility) for the given sensor and scenario conditions and $\Re(V)$ is a normalized TAWS sensor aggregate response function for detection range as a function of visibility. Note that R_{D100} is specific to a particular sensor, but that $\Re(V)$ is an average over a sensor class for a given set of atmospheric conditions. This latter qualification greatly reduces the amount of array indexing overhead. The results in equations (4) and (5) may be applied to equation (3) to yield the approximate result

$$N \cong \left(N_{50}\right)_D \frac{R_{D100}}{R} \Re(V). \tag{6}$$

This approximation of *N* may then be applied to the results in equations (1) and (2) to yield a value for the asymptotic probability of detection P_∞ under a given set of weather conditions for a specific TAWS sensor, denoted here as S1. Figure 12 compares P_∞ versus target range for S1 for two target states (exercised and inactive) and two visibilities (100 km and 2 km) using the fog aerosol. For this relatively large aerosol, visibility effects are quite pronounced. Target state is also very significant at both visibilities. Figure 13 shows the same set of conditions for the rural aerosol. The visibility is virtually insignificant in this case, due to the much smaller size parameter for

this aerosol. The applicability of the aggregate sensor response function $\Re(V)$ may also be examined by comparing it with the curve fit for S1 in figure 14. In this case, the results compare very closely for the 2 km meteorological visibility, thereby showing the applicability of using the aggregate sensor response function $\Re(V)$ in place of S1.

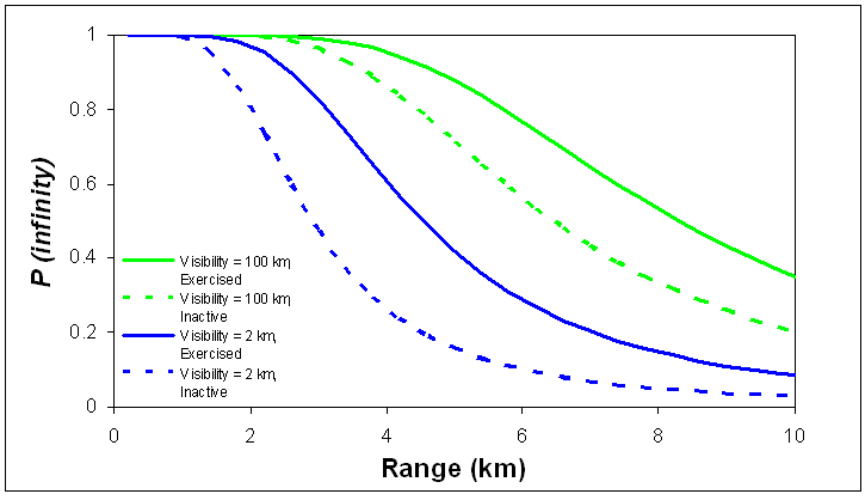

Figure 12. Asymptotic detection probability for advection fog aerosol, 0900 local time, clear sky, using a TAWS sensor.

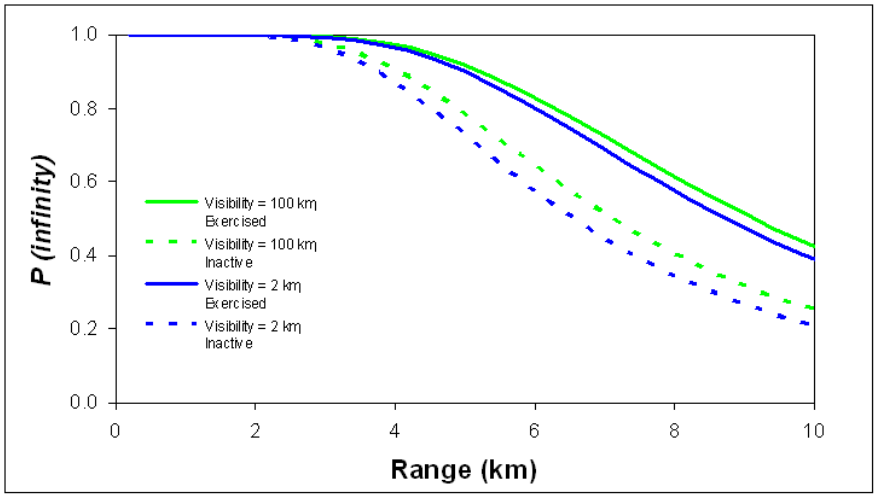

Figure 13. Detection probability for the rural aerosol, identical sensor and scenario conditions as figure 12.

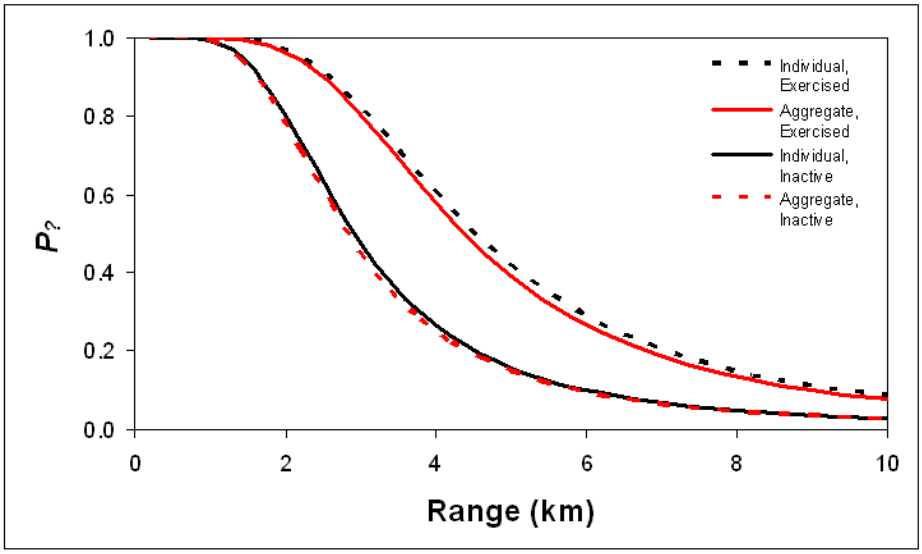

Figure 14. Sensor S1 detection probability for 2 km visibility, comparing aggregate and individual sensor response functions.

5. Critical Values/Rules

5.1 Helo and Fixed Wing Aircraft Mobility Modification

Another mechanism through which weather can affect wargame platforms is through limitation of mobility. However, it is necessary to distinguish between terrain conditions that are the result of recent weather history (for example, prolonged rains that create muddy terrain) and direct, real-time weather impacts that impose safety restrictions on platform operations (for example heavy snow that prevents fixed-wing aircraft from operating safely). While the interconnection between the long-term weather behavior and the terrain condition is important, it was beyond the scope of the work reported here. We focused instead upon direct weather effects upon airborne platforms as the most immediate means for demonstration of useful modifications to the AWARS package.

As shown previously in figure 5, the rule set interface that we developed was inserted into the helicopter libunit/helo subdirectory source code modules unit_heloresunitc2 and unit_helorequesthandler. These modules contain the vehicle mission control methods that determine whether a helicopter can initiate or continue flight operations in the presence of adverse environmental conditions. Access to the helicopter-specific rules is provided by the weather_heloIWEDArules class in the libweather subdirectory, also shown in figure 5. The weather_heloIWEDArules class is implemented as a singleton design pattern, as only a single instance of this class is needed during the course of an

AWARS simulation. When this class is instantiated, the rules data are extracted from a file named "helo_impacts.data" and are stored in vector container data members of the singleton weather_HeloIWEDARules class. These private container data members are organized by the applicable meteorological parameter and are accessed by public check methods in the unit_HeloRequestHandler and unit_HeloResUnitC2 classes. Figure 15 illustrates the dependency mechanism and execution sequence, through which the helicopter rules are employed, for the example of the unit_HeloRequestHandler class. Note that the highlighted items are not yet implemented. The last line causes the wouldUnitTypeFly method to return a Boolean 'false' value if the wind speed exceeds the IWEDA threshold for a safe takeoff for a particular helicopter platform.

```
bool unitHeloRequestHandler::wouldUnitTypeFly(const frcstr_UnitSRC & src, const terrain_Coord & faaLocation)

terrain_TerAgg * heloUnitTerAgg = faaLocation.getTerAgg();

util_Weather * weather = heloUnitTerAgg->getWeather();

testWindSpeed = weather->getWindSpeed(0.0);

weather_HeloIWEDARules * weatherRules = getHeloIWEDARules();

OTC_IList<frcstr_PlatformGroup * > platforms;

d_owner->getPlatforms( & platforms);

frcstr_PlatformGroup * platform = 0;

string platformName;

platform = platforms.item();

platformName = platform->getPlatformType()->getName();

weatherRules->checkWindSpeedRules(testWindSpeed, platformName)
```

Figure 15. Example of the IWEDA rule implementation in the unit_HeloRequestHandler class.

Instead of directly extracting weather parameter information from the native AWARS weather class interface, we inserted "hardwired" meteorological parameter values into the code. A similar work-around was used to test the DF weather effects methodology. Our implementation of the weather effects code in the unit_HeloResUnitC2 class is nearly the same as for the unit_HeloRequestHandler class. The primary difference between the two class implementations is how they use the rule set. The unit_HeloRequestHandler class, as its name implies, can force denial of requests for platform launch before a mission gets under way. The unit_HeloResUnitC2 class, on the other hand, can abort a mission that is in progress.

The rules data base that we have provided with our prototype software is limited in scope, but should be easily extended for future needs. We have included mobility and operability rules for the vehicles listed in table 3.

Table 3. Platforms included in prototype IWEDA rule data files.

Tanks	APC/AFV/IFV	FWA	Helo	Artillery
M1A1 T80 T72	M2 (Bradley) M113 BMP-1/2/3	Predator UAV	UH-1 (Huey) AH-64 (Apache) UH-60 (Blackhawk)	MLRS

The AWARS coding for the mobility methods for the FWA platforms is slightly different than that used for the helicopter platforms, so the implementation of weather effects classes for FWA platforms differs slightly as well. The FWA weather effects modifications were inserted into just the unit_FWAResUnitC2 class, and are implemented and used in much the same way as in the unit_HeloResUnitC2 class. Table 4 summarizes the classes and methods for both the helicopter and FWA platforms where the weather modifications were applied, and what actions the modifications specifically performed.

Table 4. Helicopter and FWA classes that were modified to incorporate IWEDA weather rule impacts.

Class	Method	Action
unit_HeloRequestHandler	wouldUnitTypeFly()	Accept/Deny mission request
unit_HeloResUnitC2	assessEnvironmentalConditions()	Continue/Abort mission
unit_FWAResUnitC2	assessEnvironmentalConditions()	Continue/Abort mission

5.2 Intelligence Surveillance and Reconnaissance Modifications

Since weather effects are felt most directly as limitations of mobility for airborne systems and reduction of visibility for both ground-based and airborne systems, we focused our initial modification efforts on the efficiency of DF for ground systems and the mobility of attack helicopters. The perception of the state of friendly and hostile forces on the battlefield by a given unit is also important, and is dependent upon that unit's access to ISR resources. A significant portion of the ISR function is carried out by airborne platforms (in particular, helicopters, and fixed wing aircraft), so that weather-induced mobility restrictions imposed upon these platforms (as previously described) will have repercussions for ISR.

Even more important than mobility considerations is the weather-impacted performance of ISR electro-optical sensors. Both ISR and DF sensors are similarly affected by adverse weather conditions, but have different performance implementations in AWARS. As previously discussed, the DF sensor class utilizes a resolvable cycles over target criterion to perform targeting functions. In the AWARS ISR process, a range band

probability of detection (and recognition/identification) table lookup procedure is used. The probability of detection for a given target is determined by the maximum detection range provided out of an ensemble of sensors carried by an ISR platform. Currently, this maximum range determination is obtained for each sensor in the ensemble by the getMaxDetectionRange() method of the sensorprot_SensorType class, which uses results from the sensorprot_ProbTable class. This latter class also calculates a table lookup-based probability of detection through the getProb() member function.

Though we did not implement a direct ISR probability of detection, recognition, or identification algorithm into the AWARS model, we believe that this could be achieved either by 1) modification of the sensorprot_ProbTable::getProb() method to use the DF resolvable cycles over target algorithm previously described, or 2) modifying the probability range band tables to reflect more comprehensive weather impacts. Neither of these options will be particularly easy to implement because they will both require setup of an interface to the AWARS weather class (and substantial additions to the class methods). The first option (using the DF algorithm) will likely provide the fastest and most direct interface, at the cost of greater code complexity and difficulty in modifying or expanding the sensor database. The second option will probably require less modification of existing code, but will require offline compilation of the sensor performance database to cover a wider range of weather conditions.

6. Results

Meteorological visibility effects on DF exchanges were modeled as modifications to target detection ranges for firing platforms. As previously explained, these target detection range results are curve fits derived from TAWS, aggregated within a sensor class and waveband, parameterized by aerosol type, sky cover, and TOD (among other environmental factors). The curves, which have significant execution speed advantages in many cases, are used in place of interpolated look-up tables.

To determine whether or not our methodology could improve the estimation of weather impacts in the target acquisition algorithms without increasing run time, we obtained beta versions of AWARS (*10*). We implemented systems operation rules existent in the IWEDA rule library and a set of parametric curves for target acquisition ranges. Since the AWARS code is extremely complex, we focused our efforts on weather impacts for helicopters using only IR sensors. Due to the fact that the rule and parametric curve approaches are significantly different, we found it necessary to develop a scenario where both implementations, and their effects, would be clearly delineated. Thus, the scenario that we chose was carried out under high (clear) and low (1 km) visibilities, with a blue helicopter attack on red ground forces during daylight hours under high (≥ 30 mph) and

low (< 30 mph) wind conditions, coupled with a subsequent blue ground assault on red ground forces during nighttime hours. Red was placed in a defensive position with poor night detection capability. We examined four cases:

- No Wind and Low Visibility
- No Wind and High Visibility
- High Wind and Low Visibility
- High Wind and High Visibility

To examine critical value effects, an arbitrary helicopter rule was introduced "if winds exceed 30 knots, helicopters cannot fly." Such a rule allowed us to examine whether or not there is any effect of grounding the attack helicopter on red attrition. Similarly, by allowing the ground assault to occur at night under high and low visibility conditions, coupled with red's poor night detection capability, permitted us to examine blue and red attrition under those conditions.

First we examine the high visibility case with no wind and high wind conditions. The first noticeable difference between wind and no wind is the different red attrition levels slightly after the beginning of the battle (figure 16). With high levels of wind, the blue attack helicopter is grounded, resulting in no attrition for red until the onset of the ground battle (note that, in figure 16, the blue no wind case overlays the red high wind case). Examination of figures 16–18 show the effect of the attack helicopter grounding on blue's ground forces. Both the advance blue unit (blue 1) and the secondary blue unit (blue 2) have significantly higher attrition when the attack helicopter cannot attrit any of the red force due to its being grounded under high wind conditions. Both of these effects are clear indicators that the helicopter rule is working correctly.

Turning our attention now to a detailed comparison of figures 17 and 18, high visibility vs. low visibility respectively, we can see the effects of DF attrition. This is most easily seen by comparison of the windy conditions, where the blue attack helicopter was not available. We can easily see that all blue attrition is less, while the red attrition is greater; a confirmation that our parametric sensor curve is implemented and working correctly.

It is also instructive to examine this scenario by looking at the primary units – blue 1, blue 2, and red individually under the four possible weather conditions. To that end, figures 19, 20, and 21 show the ground assault under the four weather conditions: windy, low visibility; windy, high visibility; calm, low visibility; calm, high visibility for the three ground units.

We look first at the forward deployed blue unit, blue 1 (figure 19), which has sustained the largest losses. In general, we see that this unit does better in the no wind cases, due to

the initial red attrition by the blue attack helicopter. Visibility effects on this unit are negligible in windy and calm conditions.

The situation for the secondary blue unit, blue2, is somewhat different (figure 20). Again, blue2 does better in no wind conditions when the attack helicopter is available to fly. However, again, in windy conditions blue losses are more severe. The increase in blue2 attrition in the windy, high visibility conditions towards the end of the battle is due to red subunits moving to a delay position (*11*).

Finally, we see from figure 21 that in no wind conditions, red never recovers from attrition due to the blue attack helicopter units. Overall, red does best in windy, high visibility conditions.

We constructed a second scenario where we could examine the effects of the vehicle state (off or exercised), differing visibilities (0.5, 2.0, and 25 km) in foggy conditions, and implementing a different helicopter rule–grounding of the attack helicopter by heavy rain. These results are shown in figures 22–27. While it is unlikely that any helicopter would fly in 0.5 km visibility, we have simulated such a scenario in order to heuristically examine the effects. Thus, in figure 22, we show attrition of red vehicles as a function of their state (exercised or off), due to an attack by a blue helicopter. In figure 23, the subsequent ground force attack under the same 0.5 km fog for the two vehicle states is shown. Both figures show the expected results–exercised vehicles are more easily detected and attrited. Figures 24 and 25 show red attrition for vehicles in an off state as a function of fog visibility by both the blue attack helicopter and ground forces. It may easily be seen that as the visibility increases, so does the red attrition. Finally, in figures 26 and 27, we show the effects of allowing the attack helicopter to fly or be grounded due to heavy rain, in a 2 km visibility fog on both blue and red ground units. Red does worse when the weather is clear and the blue attack helicopter can fly; blue does worse when the weather is rainy and its attack helicopter is grounded.

The purpose of these simulated battles was to show that the critical rules and the parametric sensor curves can, and do, predict realistic outcomes without incurring additional run time.

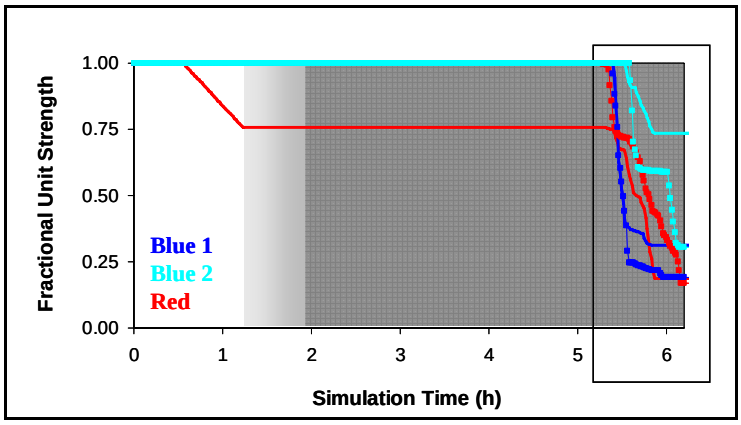

Figure 16. Blue and Red fractional attrition as a function of simulated battle time under high visibility conditions; inset is figure 17. The grey shaded area indicates nighttime; solid lines are the no wind case; lines with symbols are the high wind case.

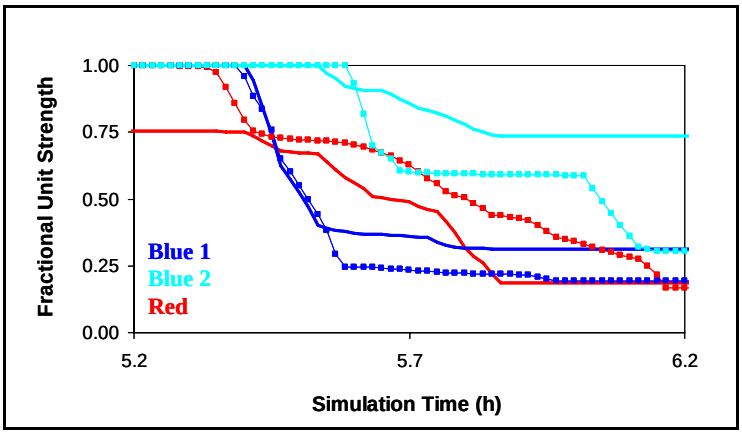

Figure 17. Inset from figure 16: Blue and Red fractional attrition as a function of simulated battle time under high visibility conditions. Line indicators are as the same as in figure 16.

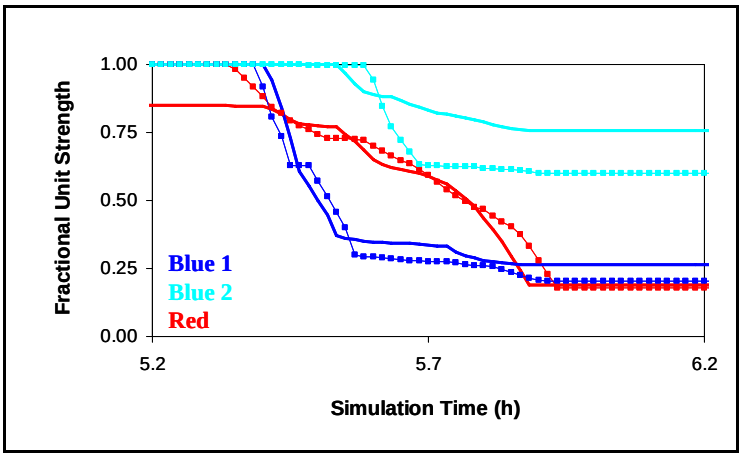

Figure 18. Blue and Red fractional attrition as a function of simulated battle time under low visibility conditions. Solid lines are the no wind case; lines with symbols are the high wind case.

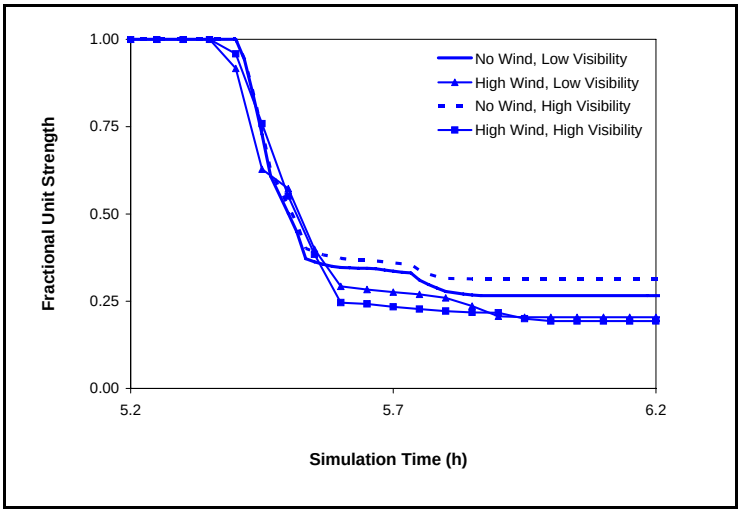

Figure 19. Blue 1 fractional attrition as a function of simulated battle time.

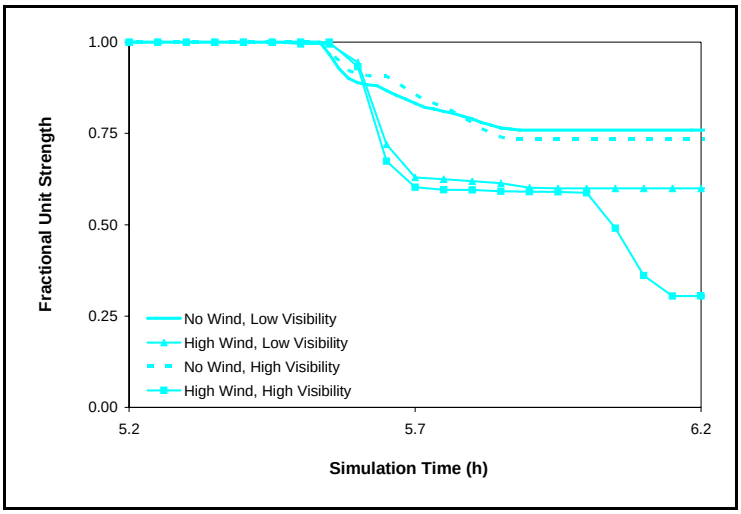

Figure 20. Blue 2 fractional attrition as a function of simulated battle time.

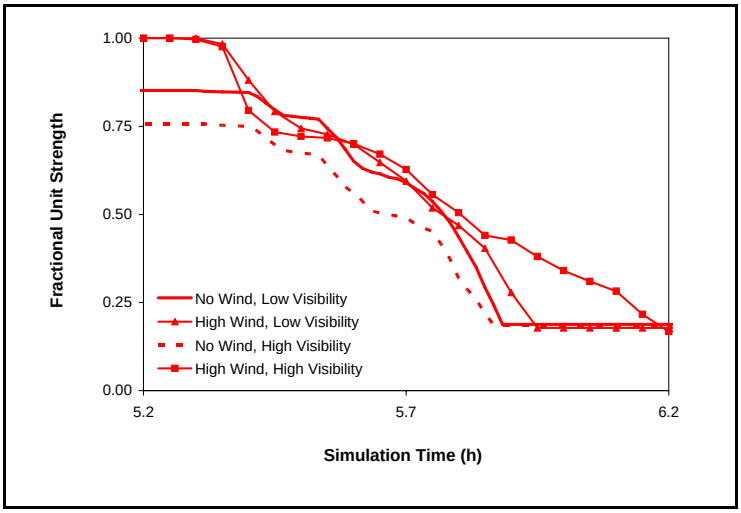

Figure 21. Red fractional attrition as a function of simulated battle time.

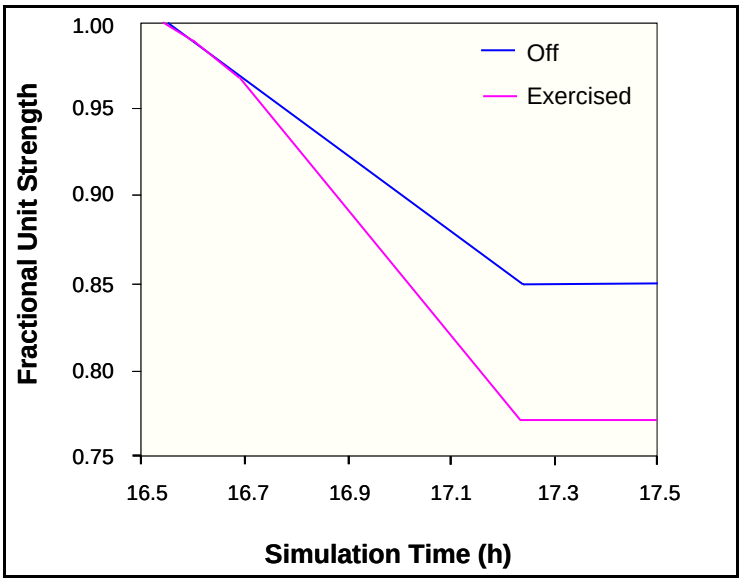

Figure 22. Red attrition as a function of vehicle state due to blue attack helicopter in a 0.5 km visibility fog.

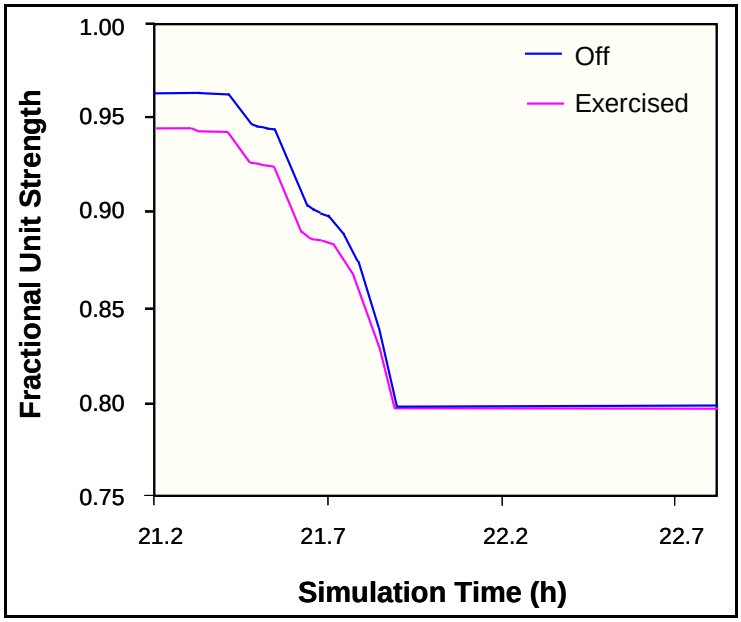

Figure 23. Red attrition as a function of vehicle state due to blue ground forces in a 0.5 km visibility fog. The blue helicopter attack has occurred previously.

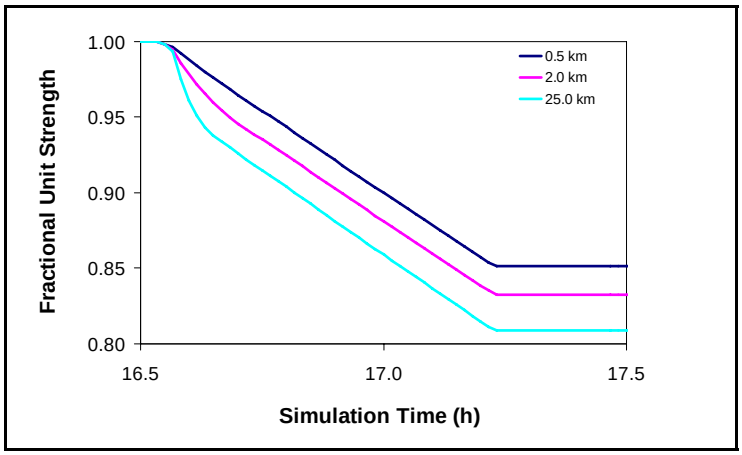

Figure 24. Red attrition from blue attack helicopter under varying visibilities.

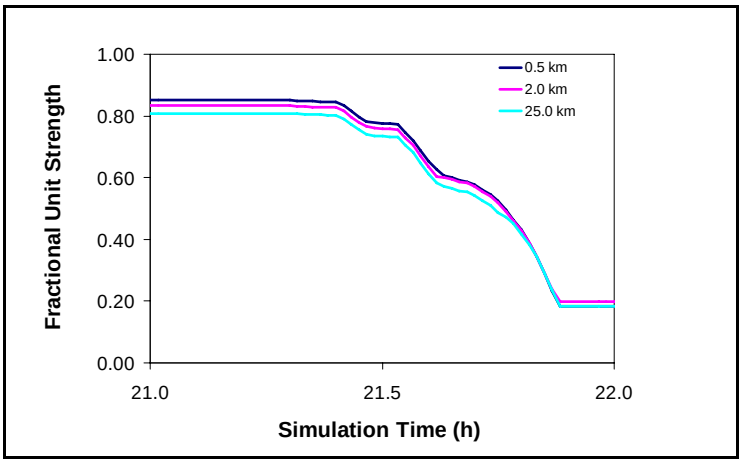

Figure 25. Red attrition from blue ground assault under varying visibilities. The attack from the blue helicopter has occurred previously.

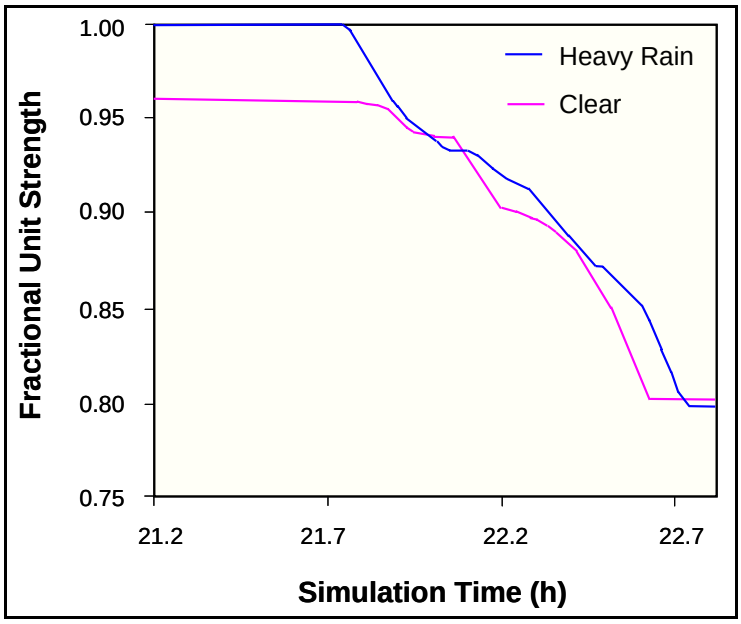

Figure 26. Red attrition from blue ground assault under a 2 km visibility. The attack helicopter was grounded due to heavy rain.

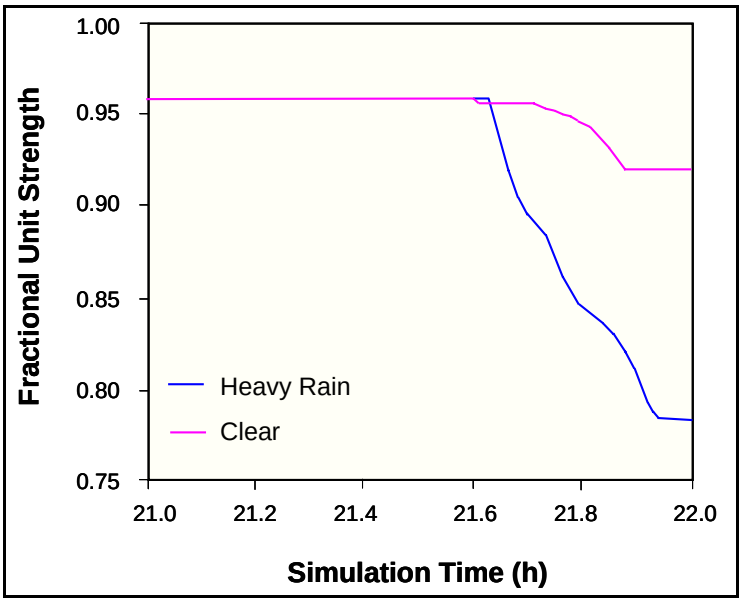

Figure 27. Blue attrition from red under a 2 km visibility. The blue attack helicopter was grounded due to heavy rain.

7. Summary and Conclusions

By familiarizing ourselves with the structure and function of the AWARS wargame we identified and exploited appropriate points where weather effects would improve the wargame realism without impacting run time. This was accomplished by implementing a treatment of DF detection processes for LWIR sensors by fitting TAWS results under different meteorological conditions to third-order polynomial curves. The execution speed of this modification compared favorably with existing table lookup methods. Second, we added interface classes and methods to the AWARS weather code library so that weather critical values, more commonly referred to as rules, could be queried under adverse weather conditions. These rules are used to determine if mobility restrictions are applicable to helicopter and fixed-wing platforms and to impose restrictions where appropriate.

The viability and significance of the DF algorithm and rules weather modifications were tested by comparing AWARS scenario evolution under optimal weather conditions with results for the same scenario under adverse weather conditions. These tests confirmed that adverse weather caused significant modification of attrition timing and levels for both ground maneuver and airborne units in a logically consistent manner.

Finally, the TAWS code and/or the constructed database and auxiliary codes, may be obtained by writing or emailing the following individual:

Army Research Laboratory
Attn: AMSRD-ARL-CI-EE (Dr. R. Shirkey)
WSMR, NM 88002-5501
rshirkey@arl.army.mil

Information regarding the critical values, or rules, database may be obtained by writing or emailing the following individual:

Army Research Laboratory
Attn: AMSRD-ARL-CI-EE (R. Szymber)
WSMR, NM 88002-5501
rszymber@arl.army.mil

References

1. *Warfare Modeling*, Bracken, J., M Kress, R.E. Rosenthal, Eds.; John Wiley & Sons, Inc., 1995.
2. http://www.amso.army.mil/sim-sys/ (access verified as of 17 October 2006).
3. http://www.msrr.army.mil/ (access verified as of 17 October 2006).
4. http://www.msrr.dmso.mil/ (access verified as of 17 October 2006).
5. http://afmsrr.afams.af.mil (access verified as of 17 October 2006).
6. Shirkey, R.C.; Gouveia M. Weather Impact Decision Aids: Software to Help Plan for Optimal Sensor and System Performance. *Crosstalk*, the Journal of Defense Software Engineering. **2002,** *15*, No. 12, 17–21.
7. *ACQUIRE Range Performance Model for Target Acquisition Systems 1995, Version 1 User's Guide*, U.S. Army CECOM Night Vision and Electronic Sensors Directorate Report: Ft. Belvoir, VA, May 1995.
8. Press, W.H.; Teukolsky, S.A.; Vetterling, W. T.; Flannery, B.P. *Numerical Recipes in Fortran 77: the art of scientific computing*, 2nd ed ., pp 113–115, Cambridge University Press: New York, NY, 2003.
9. Howe, J.D. Chapter 2: Electro-Optical Imaging System Performance Prediction. In *The Infrared and Electro-Optical Systems Handbook*, Vol 4, Electro-Optical Systems Design, Analysis, and Testing; Dudzik M.C., Ed.; SPIE Optical Engineering Press: Bellingham, WA, 1993.
10. Gach, T. and S. R. Glasgow. Private communications, 2000-2004.
11. Shirkey, R.C.; O'Brien, S.G. *Modification of the Weather Effects Implementation in the AWARS Model*, in proceedings of the 72nd Military Operations Research Society Symposium: Monterey, CA, 23 June 2004.

INTENTIONALLY LEFT BLANK.

Appendix A. Representative Rule Classes for Army, Navy (Marines) and Air Force

Operations, systems, sub-systems and components on the same row are independent and not linked. Note that, a system could be a helicopter, its sub-system could be an engine, and an engine component could be a turboshaft. However, if the system is considered to be the engine, then the turboshaft would be a sub-system; a low horsepower engine could be a component of some larger system; a missile launcher system could have the missile as a sub-system and the missile's sensor as a component. The Integrated Weather Effects Decision Aid (IWEDA) provides an easy method for delineating this structure.

Table A-1. Representative Army rule classes for operations, systems, sub-systems, and components.

Army			
Operations	**Systems**	**Sub-Systems**	**Components**
Aerial Forward Observer	Aerostat	Aerial recovery	Acoustic sensors
Air assault	Aircraft (all)	Aerostat (platform)	Ammunition
Air attack	Amphibious assault vehicle	Ammunition	Antenna
Air refueling	Laser IR observation set	Chain gun	Artillery fuzes
Airborne airdrop	Night vision goggles	Collapsible water tank	Aviation gasoline
Aircraft (fixed- and rotary-wing)	Night vision sights	Engines	Batteries
Aircraft Landing	Personnel – cold/heat Injuries	Gatling gun	Diesel engine
Amphibious	Tanker	Generators	Fuels & Gasolines (all)
Arming/Rearming	Target pointer illuminator	Guided bombs	Grease
Bombing	Truck	High Explosive Anti-Tank (HEAT) warheads	High Frequency (HF) Interceptor
Bridging	Unmanned Aerial Vehicle	Hydraulic pumps	HF Jammer
Combat Search & Rescue		Personnel	HF Radio

Army			
Operations	**Systems**	**Sub-Systems**	**Components**
Concealment and Camouflage		Magazines	Munitions
Cross-country movement mobility		Micro air vehicles	Rockets
Field artillery		Mission payloads	Hydraulic O-Ring Seals
Fording		Mission Payload Sensors	Hydraulic Systems
Fueling/refueling		Missiles	Jet Fuel
Ground maneuver		Mortar rounds	Launcher
Logistics		Night sights	Lubricants
Medical		Night Vision Goggles	Military Standard Gasoline Engine
Mortar		Rotors (main, all types)	Mines
Night vision goggles		Rockets	Missiles
Ordinance		Unmanned Aerial Vehicles	Plastic Explosives
River crossing			Portable Rugged Personal Computer
Unmanned Aerial Vehicle			Uninterruptible Power Supply

Table A-2. Representative Navy rule classes for operations, systems, sub-systems, and components.

Navy			
Operations	**Systems**	**Sub-Systems**	**Components**
Aerial resonance	Boats	Aerial mines	Acquisition radar
Air defense	Fixed Wing	Ammunition	Ammunition
Aircraft carrier	Flight operations	Antennas	Cannons
Airborne	Helicopters	Bombs	IR guidance
Airdrop Operations	Personnel	Cruise missiles	IR seekers
Airborne refueling	Surface to air missiles	Fuels	Launchers
Amphibious	Tracked vehicles	Grenade launchers	Radar
Aviation	Unmanned aerial vehicles	Missiles	Thermal sights
Engineer	Wheeled vehicles	Mortars	TV guidance
Ground maneuver		Night vision goggles	
Helicopter		Personnel maintenance	
Intelligence		Personnel swimmer/diver	
Signal Communications		Rocket launchers	
Sub-Surface		Navigation radars	
Surface ships		Thermal viewers	

Table A-3. Representative Air Force rule classes for systems.

Air Force
Systems
Aircraft

A Special Note about Monikers used in Appendices B and C

Table A-4 applies to both appendices B and C.

Each moniker, used in the following table, is a concatenation of the various atmospheric conditions that we used; with the exception of the 0900 time period, the first three characters of each atmospheric condition were used. This cipher is presented in table A-4.

Table A-4. Monikers and their meaning as used in the various tables and figures in appendices B and C.

Moniker	Meaning
Fog	Fog
Rur	Rural
Tan	Tank
Exe	Exercised
Off	Inactive
900	0900
150	1500
Win	Winter
Sum	Summer
Nor	North
Sou	South
Eas	East
Wes	West
Ove	Overcast
Cle	Clear

Appendix B. Third-Order Polynomial Coefficients and their Curves for the Fog Aerosol for a NFOV and WFOV Average IR Sensor

Table B-1. Third-order polynomial coefficients curve fit to averaged quantities as represented by moniker for average sensor viewing through a fog aerosol. WFOV results are shown.

Moniker	a0	a1	a2	a3	Average Maximum Detection Range
150CleFog	0.721	0.355	-0.056	-0.026	3.59
150OveFog	0.707	0.364	-0.048	-0.030	3.59
900CleFog	0.619	0.398	0.001	-0.052	3.42
900OveFog	0.545	0.406	0.038	-0.063	3.25
Tan900CleFog	0.711	0.343	-0.051	-0.024	2.69
Tan150CleFog	0.813	0.282	-0.106	0.006	2.80
Tan900OveFog	0.668	0.363	-0.027	-0.036	2.68
Tan150OveFog	0.805	0.289	-0.102	0.003	2.79
TanExe150OveFog	0.830	0.270	-0.118	0.013	2.81
TanExe900OveFog	0.763	0.323	-0.080	-0.011	2.78
TanExe150CleFog	0.830	0.269	-0.116	0.012	2.82
TanExe900CleFog	0.773	0.314	-0.084	-0.008	2.78
TanOff900CleFog	0.634	0.379	-0.009	-0.044	2.58
TanOff150CleFog	0.795	0.295	-0.096	0.000	2.78
TanOff150OveFog	0.779	0.308	-0.086	-0.006	2.76
TanOff900OveFog	0.557	0.409	0.035	-0.065	2.56
TanOff900SumOveFog	0.564	0.406	0.030	-0.062	2.45
TanOff900WinOveFog	0.524	0.422	0.055	-0.074	2.63
TanOff150SumOveFog	0.795	0.294	-0.094	-0.001	2.77
TanOff150WinOveFog	0.732	0.349	-0.065	-0.021	2.74
TanOff900NorOveFog	0.547	0.402	0.036	-0.062	2.51
TanOff900EasOveFog	0.524	0.402	0.053	-0.068	2.44
TanOff900WesOveFog	0.611	0.416	0.012	-0.061	2.66
TanOff900SouOveFog	0.539	0.414	0.043	-0.067	2.60
TanExe900SumOveFog	0.763	0.323	-0.080	-0.011	2.78
TanExe900WinOveFog	0.757	0.330	-0.078	-0.013	2.79
TanExe150SumOveFog	0.835	0.265	-0.120	0.014	2.81
TanExe150WinOveFog	0.811	0.289	-0.111	0.007	2.81
TanExe900NorOveFog	0.843	0.264	-0.128	0.018	2.85
TanExe900EasOveFog	0.746	0.337	-0.072	-0.017	2.76
TanExe900WesOveFog	0.769	0.319	-0.087	-0.008	2.78
TanExe900SouOveFog	0.695	0.371	-0.034	-0.038	2.72
TanExe150NorOveFog	0.860	0.249	-0.136	0.023	2.85
TanExe150EasOveFog	0.833	0.267	-0.121	0.014	2.81
TanExe150WesOveFog	0.832	0.268	-0.118	0.013	2.81
TanExe150SouOveFog	0.795	0.296	-0.098	0.001	2.78
TanExe900NorCleFog	0.846	0.262	-0.131	0.019	2.85
TanExe900EasCleFog	0.748	0.337	-0.075	-0.015	2.76

Moniker	a0	a1	a2	a3	Average Maximum Detection Range
TanExe900WesCleFog	0.810	0.283	-0.102	0.004	2.81
TanExe900SouCleFog	0.688	0.374	-0.028	-0.041	2.72
TanExe150NorCleFog	0.865	0.244	-0.138	0.025	2.85
TanExe150EasCleFog	0.847	0.255	-0.125	0.018	2.83
TanExe150WesCleFog	0.817	0.279	-0.109	0.007	2.80
TanExe150SouCleFog	0.792	0.297	-0.093	-0.002	2.79
TanOff900NorCleFog	0.607	0.402	0.006	-0.054	2.49
TanOff900EasCleFog	0.542	0.408	0.042	-0.066	2.40
TanOff900WesCleFog	0.775	0.315	-0.091	-0.005	2.77
TanOff900SouCleFog	0.561	0.415	0.035	-0.066	2.59
TanOff150NorCleFog	0.789	0.300	-0.090	-0.003	2.77
TanOff150EasCleFog	0.832	0.269	-0.122	0.015	2.80
TanOff150WesCleFog	0.789	0.301	-0.092	-0.003	2.77
TanOff150SouCleFog	0.771	0.312	-0.079	-0.010	2.76
TanOff900SumNorCleFog	0.524	0.358	0.029	-0.045	2.07
TanOff900SumEasCleFog	0.541	0.384	0.022	-0.050	2.58
TanOff900SumWesCleFog	0.778	0.315	-0.098	-0.002	2.78
TanOff900SumSouCleFog	0.578	0.431	0.031	-0.071	2.70
TanOff150SumNorCleFog	0.779	0.306	-0.083	-0.007	2.75
TanOff150SumEasCleFog	0.840	0.264	-0.128	0.018	2.80
TanOff150SumWesCleFog	0.802	0.288	-0.098	0.002	2.78
TanOff150SumSouCleFog	0.806	0.286	-0.102	0.004	2.78
TanOff900WinNorCleFog	0.651	0.405	-0.010	-0.053	2.72
TanOff90Win0EasCleFog	0.595	0.442	0.024	-0.072	2.69
TanOff900WinWesCleFog	0.763	0.331	-0.092	-0.007	2.77
TanOff900WinSouCleFog	0.549	0.403	0.036	-0.062	2.78
TanOff150WinNorCleFog	0.793	0.300	-0.096	-0.001	2.81
TanOff150WinEasCleFog	0.810	0.286	-0.105	0.005	2.79
TanOff150WinWesCleFog	0.747	0.339	-0.074	-0.016	2.75
TanOff150WinSouCleFog	0.690	0.374	-0.029	-0.040	2.74
TanExe900SumNorCleFog	0.840	0.266	-0.125	0.016	2.85
TanExe900SumEasCleFog	0.737	0.344	-0.066	-0.020	2.75
TanExe900SumWesCleFog	0.809	0.282	-0.100	0.003	2.81
TanExe900SumSouCleFog	0.709	0.361	-0.044	-0.032	2.74
TanExe150SumNorCleFog	0.864	0.244	-0.138	0.025	2.85
TanExe150SumEasCleFog	0.846	0.254	-0.122	0.017	2.82
TanExe150SumWesCleFog	0.819	0.277	-0.110	0.008	2.80
TanExe150SumSouCleFog	0.810	0.281	-0.101	0.004	2.80
TanExe900WinNorCleFog	0.866	0.254	-0.147	0.027	2.85
TanExe90Win0EasCleFog	0.776	0.322	-0.100	-0.003	2.78
TanExe900WinWesCleFog	0.810	0.287	-0.105	0.004	2.82
TanExe900WinSouCleFog	0.680	0.380	-0.023	-0.044	2.75
TanExe150WinNorCleFog	0.876	0.244	-0.149	0.029	2.85
TanExe150WinEasCleFog	0.844	0.263	-0.129	0.018	2.85
TanExe150WinWesCleFog	0.809	0.287	-0.104	0.004	2.81
TanExe150WinSouCleFog	0.739	0.343	-0.069	-0.019	2.76
TanOff900SumNorOveFog	0.545	0.385	0.032	-0.055	2.01

Moniker	a0	a1	a2	a3	Average Maximum Detection Range
TanOff900SumEasOveFog	0.505	0.396	0.064	-0.069	2.28
TanOff900SumWesOveFog	0.642	0.416	-0.011	-0.054	2.67
TanOff900SumSouOveFog	0.532	0.411	0.047	-0.068	2.53
TanOff150SumNorOveFog	0.779	0.308	-0.087	-0.006	2.74
TanOff150SumEasOveFog	0.810	0.282	-0.103	0.005	2.78
TanOff150SumWesOveFog	0.810	0.284	-0.104	0.005	2.78
TanOff150SumSouOveFog	0.780	0.304	-0.082	-0.007	2.76
TanOff900WinNorOveFog	0.544	0.408	0.037	-0.063	2.69
TanOff900Win0EasOveFo	0.520	0.428	0.063	-0.078	2.53
TanOff900WinWesOveFog	0.516	0.432	0.068	-0.081	2.62
TanOff900WinSouOveFog	0.521	0.415	0.044	-0.066	2.74
TanOff150WinNorOveFog	0.739	0.346	-0.073	-0.017	2.74
TanOff150WinEasOveFog	0.747	0.339	-0.075	-0.016	2.74
TanOff150WinWesOveFog	0.743	0.342	-0.072	-0.017	2.74
TanOff150WinSouOveFog	0.699	0.368	-0.039	-0.035	2.73
TanExe900SumNorOveFog	0.840	0.266	-0.125	0.016	2.85
TanExe900SumEasOveFog	0.743	0.340	-0.072	-0.017	2.77
TanExe900SumWesOveFog	0.779	0.312	-0.092	-0.004	2.78
TanExe900SumSouOveFog	0.692	0.373	-0.031	-0.039	2.71
TanExe150SumNorOveFog	0.855	0.250	-0.131	0.021	2.85
TanExe150SumEasOveFog	0.840	0.261	-0.125	0.017	2.81
TanExe150SumWesOveFog	0.836	0.264	-0.123	0.016	2.81
TanExe150SumSouOveFog	0.807	0.285	-0.101	0.003	2.78
TanExe900WinNorOveFog	0.855	0.261	-0.138	0.022	2.85
TanExe900WinEasOveFog	0.745	0.340	-0.075	-0.016	2.78
TanExe900WinWesOveFog	0.745	0.340	-0.075	-0.016	2.78
TanExe900WinSouOveFog	0.683	0.379	-0.025	-0.043	2.75
TanExe150WinNorOveFog	0.866	0.253	-0.146	0.026	2.85
TanExe150WinEasOveFog	0.813	0.284	-0.108	0.006	2.81
TanExe150WinWesOveFog	0.809	0.287	-0.104	0.004	2.81
TanExe150WinSouOveFog	0.756	0.333	-0.084	-0.011	2.77

Table B-2. Third-order polynomial coefficients curve fit to averaged quantities as represented by moniker for average sensor viewing through a fog aerosol. NFOV results are shown. Coefficients in blue have associated curves presented in the graphs in this appendix.

Moniker	a0	a1	a2	a3	Average Maximum Detection Range
150CleFog	0.323	0.606	0.211	-0.172	8.88
150OveFog	0.313	0.604	0.215	-0.173	8.88
900CleFog	0.270	0.574	0.223	-0.164	8.52
900OveFog	0.243	0.511	0.206	-0.136	8.22
Tan900CleFog	0.316	0.579	0.200	-0.159	7.59
Tan150CleFog	0.381	0.598	0.176	-0.160	7.80
Tan900OveFog	0.295	0.556	0.200	-0.151	7.62
Tan150OveFog	0.372	0.602	0.183	-0.164	7.80
TanExe150OveFog	0.394	0.593	0.166	-0.156	7.80
TanExe900OveFog	0.344	0.610	0.199	-0.170	7.80
TanExe150CleFog	0.400	0.590	0.162	-0.153	7.80
TanExe900CleFog	0.352	0.604	0.192	-0.166	7.80
TanOff900CleFog	0.271	0.548	0.209	-0.151	7.32
TanOff150CleFog	0.363	0.606	0.190	-0.167	7.80
TanOff150OveFog	0.351	0.612	0.200	-0.172	7.80
TanOff900OveFog	0.235	0.491	0.201	-0.128	7.39
TanOff900SumOveFog	0.235	0.489	0.200	-0.127	7.20
TanOff900WinOveFog	0.217	0.520	0.225	-0.144	8.02
TanOff150SumOveFog	0.360	0.602	0.192	-0.166	7.80
TanOff150WinOveFog	0.319	0.642	0.229	-0.190	7.80
TanOff900NorOveFog	0.225	0.480	0.200	-0.123	7.30
TanOff900EasOveFog	0.232	0.472	0.195	-0.119	7.02
TanOff900WesOveFog	0.249	0.523	0.210	-0.142	7.80
TanOff900SouOveFog	0.229	0.479	0.199	-0.123	7.36
TanExe900SumOveFog	0.344	0.612	0.201	-0.172	7.80
TanExe900WinOveFog	0.350	0.624	0.201	-0.175	7.80
TanExe150SumOveFog	0.397	0.590	0.164	-0.154	7.80
TanExe150WinOveFog	0.384	0.604	0.173	-0.160	7.80
TanExe900NorOveFog	0.408	0.589	0.154	-0.150	7.80
TanExe900EasOveFog	0.334	0.623	0.210	-0.178	7.80
TanExe900WesOveFog	0.343	0.621	0.206	-0.176	7.80
TanExe900SouOveFog	0.291	0.606	0.227	-0.176	7.80
TanExe150NorOveFog	0.424	0.577	0.142	-0.143	7.80
TanExe150EasOveFog	0.400	0.592	0.162	-0.154	7.80
TanExe150WesOveFog	0.391	0.595	0.169	-0.157	7.80
TanExe150SouOveFog	0.360	0.609	0.192	-0.168	7.80
TanExe900NorCleFog	0.409	0.588	0.153	-0.149	7.80
TanExe900EasCleFog	0.327	0.623	0.215	-0.179	7.80
TanExe900WesCleFog	0.386	0.601	0.173	-0.160	7.80
TanExe900SouCleFog	0.288	0.603	0.228	-0.176	7.80
TanExe150NorCleFog	0.428	0.574	0.139	-0.142	7.80
TanExe150EasCleFog	0.418	0.580	0.148	-0.146	7.80
TanExe150WesCleFog	0.390	0.596	0.170	-0.157	7.80
TanExe150SouCleFog	0.365	0.608	0.189	-0.167	7.80
TanOff900NorCleFog	0.246	0.536	0.216	-0.147	7.10

Moniker	a0	a1	a2	a3	Average Maximum Detection Range
TanOff900EasCleFog	0.237	0.504	0.208	-0.134	6.79
TanOff900WesCleFog	0.346	0.621	0.206	-0.177	7.80
TanOff900SouCleFog	0.229	0.504	0.209	-0.134	7.36
TanOff150NorCleFog	0.354	0.606	0.196	-0.169	7.80
TanOff150EasCleFog	0.393	0.595	0.168	-0.157	7.80
TanOff150WesCleFog	0.358	0.608	0.193	-0.168	7.80
TanOff150SouCleFog	0.345	0.615	0.204	-0.174	7.80
TanOff900SumNorCleFog	0.207	0.442	0.189	-0.106	6.23
TanOff900SumEasCleFog	0.237	0.471	0.184	-0.114	7.39
TanOff900SumWesCleFog	0.345	0.624	0.208	-0.178	7.80
TanOff900SumSouCleFog	0.230	0.518	0.215	-0.141	7.70
TanOff150SumNorCleFog	0.344	0.603	0.203	-0.170	7.80
TanOff150SumEasCleFog	0.396	0.591	0.166	-0.155	7.80
TanOff150SumWesCleFog	0.366	0.600	0.186	-0.164	7.80
TanOff150SumSouCleFog	0.367	0.600	0.186	-0.164	7.80
TanOff900WinNorCleFog	0.271	0.651	0.260	-0.202	7.80
TanOff90Win0EasCleFog	0.242	0.594	0.248	-0.178	7.80
TanOff900WinWesCleFog	0.340	0.630	0.209	-0.180	7.80
TanOff900WinSouCleFog	0.224	0.543	0.228	-0.153	8.43
TanOff150WinNorCleFog	0.362	0.615	0.195	-0.171	7.80
TanOff150WinEasCleFog	0.381	0.605	0.176	-0.162	7.80
TanOff150WinWesCleFog	0.334	0.633	0.216	-0.183	7.80
TanOff150WinSouCleFog	0.291	0.655	0.250	-0.200	7.80
TanExe900SumNorCleFog	0.403	0.592	0.157	-0.152	7.80
TanExe900SumEasCleFog	0.318	0.632	0.223	-0.184	7.80
TanExe900SumWesCleFog	0.384	0.602	0.175	-0.161	7.80
TanExe900SumSouCleFog	0.300	0.633	0.237	-0.189	7.80
TanExe150SumNorCleFog	0.421	0.578	0.146	-0.145	7.80
TanExe150SumEasCleFog	0.418	0.579	0.150	-0.147	7.80
TanExe150SumWesCleFog	0.391	0.594	0.169	-0.157	7.80
TanExe150SumSouCleFog	0.379	0.599	0.178	-0.161	7.80
TanExe900WinNorCleFog	0.430	0.576	0.133	-0.139	7.80
TanExe90Win0EasCleFog	0.347	0.627	0.203	-0.176	7.80
TanExe900WinWesCleFog	0.386	0.602	0.171	-0.159	7.80
TanExe900WinSouCleFog	0.289	0.658	0.253	-0.202	7.80
TanExe150WinNorCleFog	0.444	0.567	0.124	-0.134	7.80
TanExe150WinEasCleFog	0.414	0.584	0.149	-0.147	7.80
TanExe150WinWesCleFog	0.383	0.604	0.174	-0.161	7.80
TanExe150WinSouCleFog	0.331	0.635	0.218	-0.184	7.80
TanOff900SumNorOveFog	0.218	0.460	0.192	-0.113	6.02
TanOff900SumEasOveFog	0.225	0.445	0.182	-0.105	7.21
TanOff900SumWesOveFog	0.258	0.546	0.217	-0.152	7.80
TanOff900SumSouOveFog	0.225	0.470	0.198	-0.120	7.19
TanOff150SumNorOveFog	0.344	0.602	0.202	-0.170	7.80
TanOff150SumEasOveFog	0.379	0.599	0.178	-0.161	7.80
TanOff150SumWesOveFog	0.368	0.602	0.186	-0.164	7.80
TanOff150SumSouOveFog	0.347	0.603	0.200	-0.169	7.80
TanOff900WinNorOveFog	0.214	0.521	0.227	-0.146	8.58
TanOff900Win0EasOveFo	0.212	0.505	0.221	-0.138	7.66

Moniker	a0	a1	a2	a3	Average Maximum Detection Range
TanOff900WinWesOveFog	0.218	0.529	0.228	-0.148	7.79
TanOff900WinSouOveFog	0.225	0.528	0.223	-0.146	8.43
TanOff150WinNorOveFog	0.318	0.643	0.230	-0.190	7.80
TanOff150WinEasOveFog	0.333	0.634	0.217	-0.183	7.80
TanOff150WinWesOveFog	0.327	0.637	0.222	-0.186	7.80
TanOff150WinSouOveFog	0.296	0.655	0.247	-0.199	7.80
TanExe900SumNorOveFog	0.406	0.589	0.156	-0.151	7.80
TanExe900SumEasOveFog	0.332	0.628	0.215	-0.181	7.80
TanExe900SumWesOveFog	0.347	0.623	0.206	-0.177	7.80
TanExe900SumSouOveFog	0.290	0.608	0.229	-0.178	7.80
TanExe150SumNorOveFog	0.420	0.579	0.147	-0.146	7.80
TanExe150SumEasOveFog	0.405	0.588	0.158	-0.151	7.80
TanExe150SumWesOveFog	0.394	0.591	0.167	-0.156	7.80
TanExe150SumSouOveFog	0.368	0.600	0.185	-0.163	7.80
TanExe900WinNorOveFog	0.424	0.580	0.138	-0.142	7.80
TanExe900WinEasOveFog	0.344	0.628	0.206	-0.178	7.80
TanExe900WinWesOveFog	0.342	0.629	0.208	-0.179	7.80
TanExe900WinSouOveFog	0.290	0.657	0.252	-0.202	7.80
TanExe150WinNorOveFog	0.435	0.574	0.128	-0.137	7.80
TanExe150WinEasOveFog	0.386	0.602	0.171	-0.159	7.80
TanExe150WinWesOveFog	0.382	0.604	0.175	-0.161	7.80
TanExe150WinSouOveFog	0.333	0.634	0.217	-0.184	7.80

The coefficients displayed in blue in table B-2 have associated curves that are presented in the following graphs labeled figures B-1 through B-15.

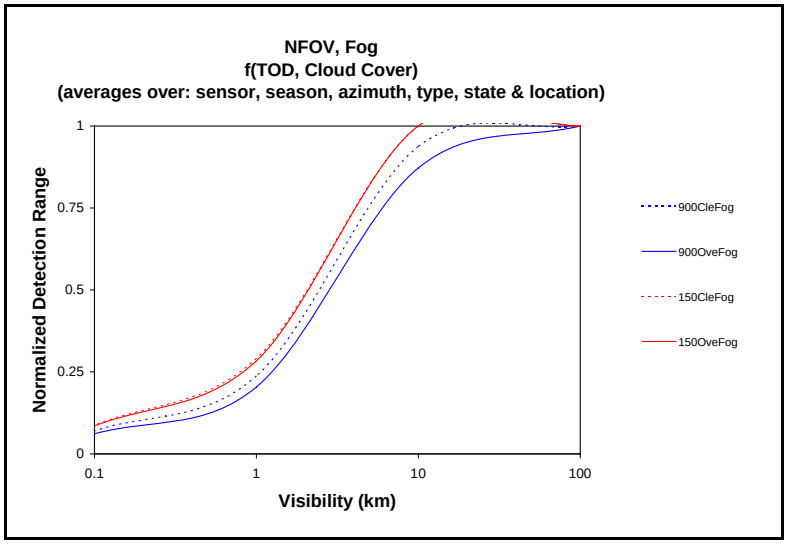

Figure B-1. Normalized detection range vs. visibility for a NFOV average sensor in a fog aerosol as a function of TOD and cloud cover. Averages were taken over seasons, locations, azimuths, target types and operating states, as presented in table B-2.

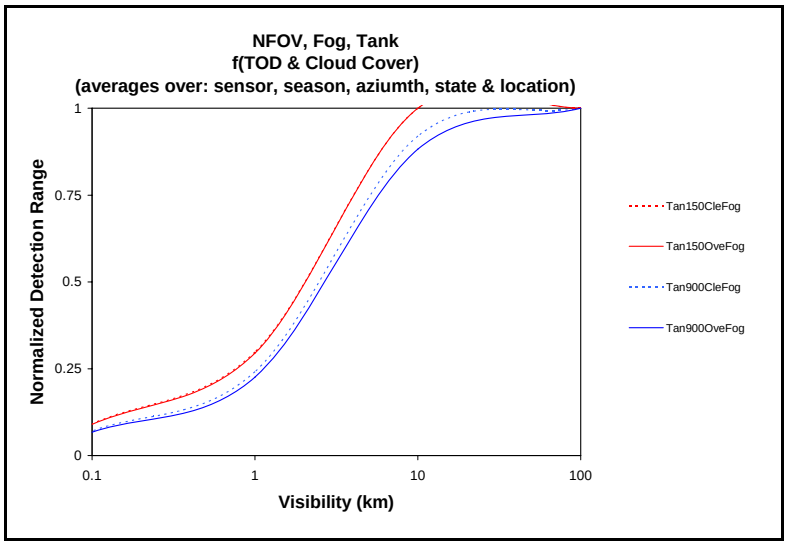

Figure B-2. Normalized detection range vs. visibility for a NFOV average sensor, in a fog aerosol, viewing a tank, as a function of time of day and cloud cover. Averages were taken over seasons, locations, azimuths, and target operating states, as presented in table B-2.

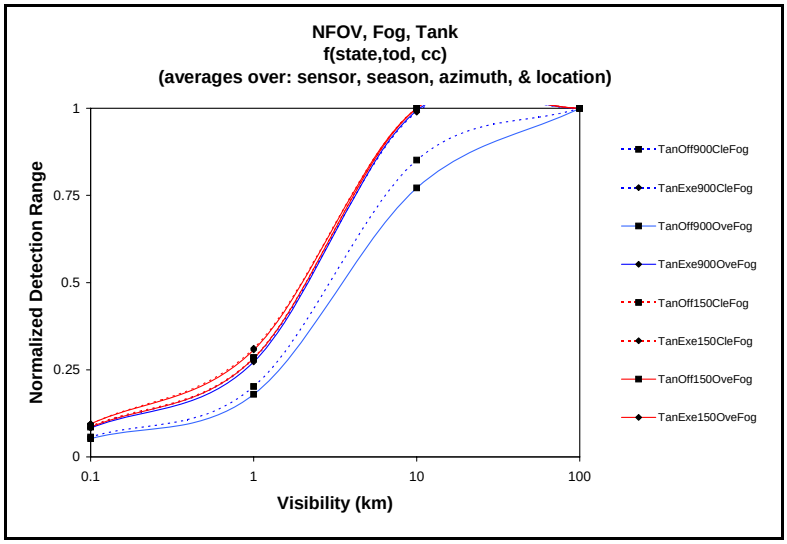

Figure B-3. Normalized detection range vs. visibility for a NFOV average sensor in a fog aerosol as a function of target operating state, time of day and cloud cover. Averages were taken over seasons, locations, and azimuths, as presented in table B-2.

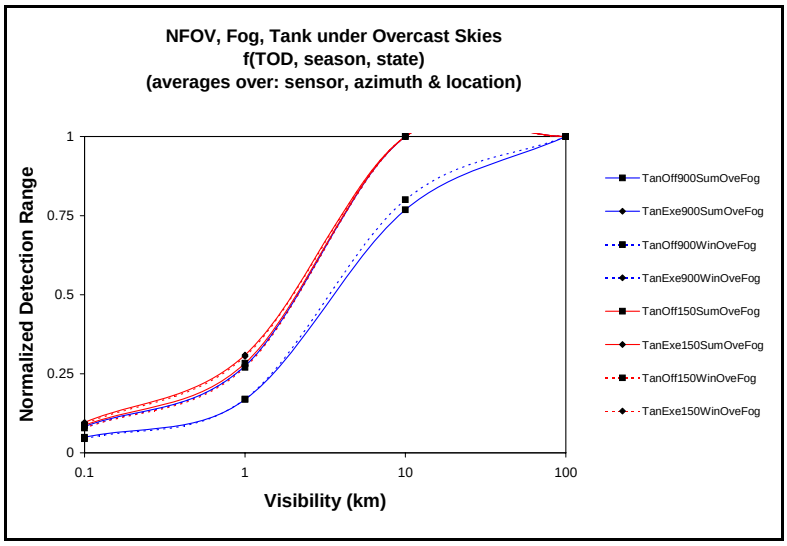

Figure B-4. Normalized detection range vs. visibility for a NFOV average sensor, in a fog aerosol, viewing a tank under overcast skies, as a function of TOD, season, and operating state. Averages were taken over locations, and azimuths, as presented in table B-2.

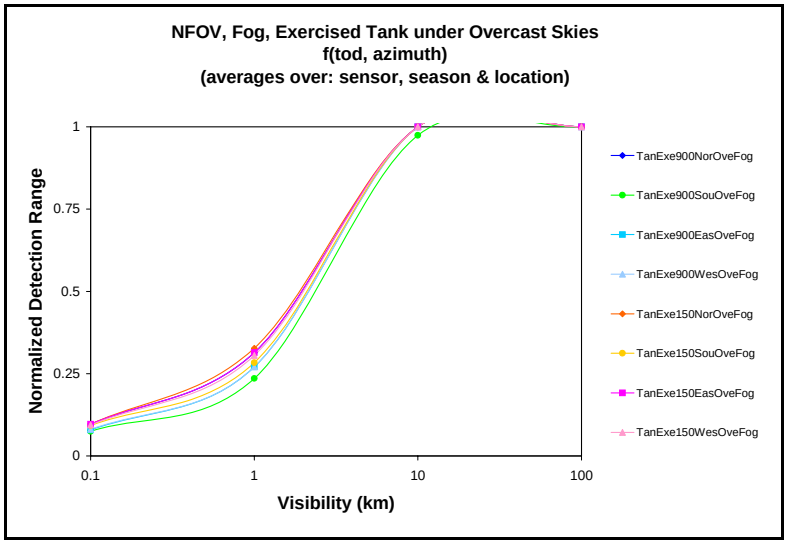

Figure B-5. Normalized detection range vs. visibility for a NFOV average sensor in a fog aerosol viewing an exercised tank under overcast skies as a function of TOD and azimuth. Averages were taken over seasons and locations, as presented in table B-2.

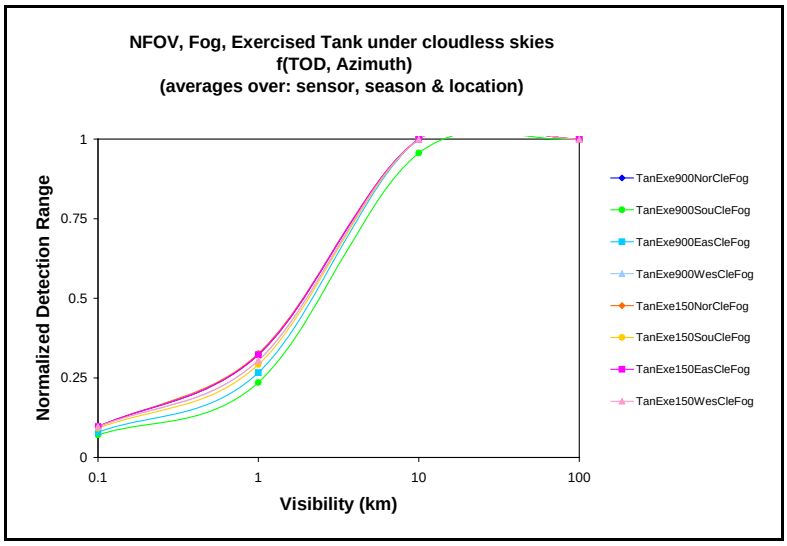

Figure B-6. Normalized detection range vs. visibility for a NFOV average sensor, in a fog aerosol, viewing an exercised tank under clear skies, as a function of TOD, and azimuth. Averages were taken over seasons and locations, as presented in table B-2.

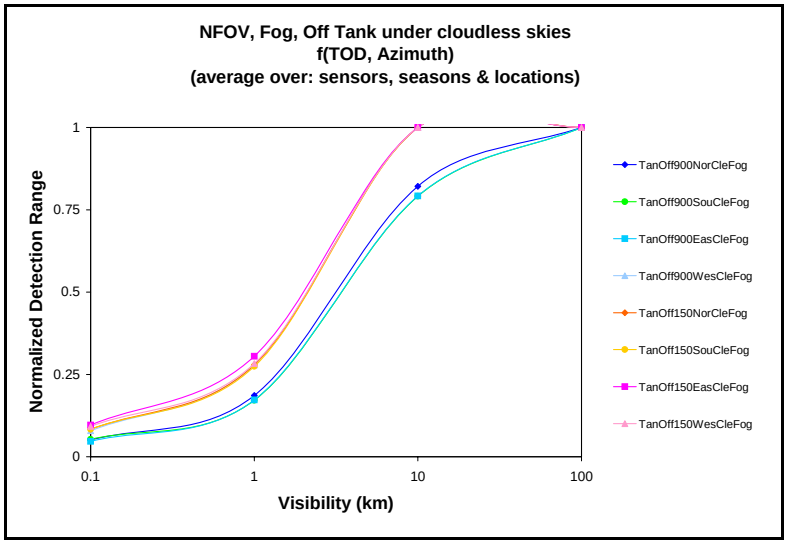

Figure B-7. Normalized detection range vs. visibility for a NFOV average sensor in a fog aerosol viewing an inactive tank under clear skies as a function of TOD and azimuth. Averages were taken over seasons and locations, as presented in table B-2.

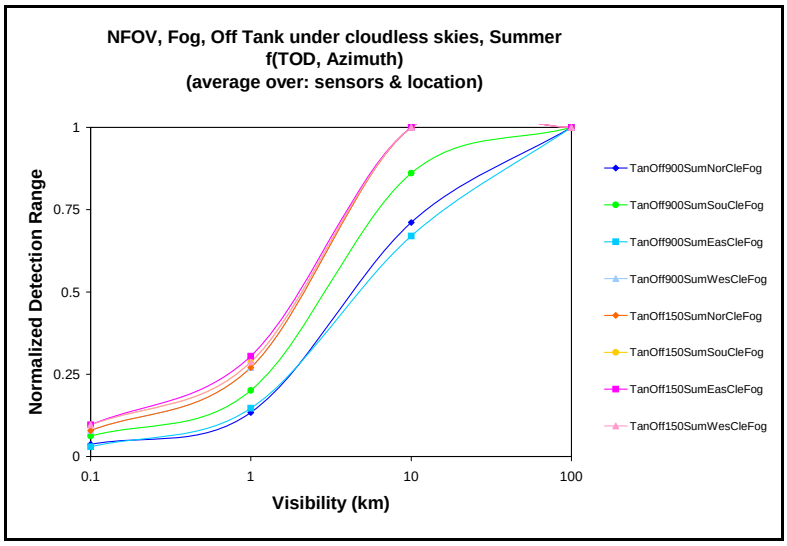

Figure B-8. Normalized detection range vs. visibility for a NFOV average sensor, in a fog aerosol, viewing an inactive tank under clear skies in the summer, as a function of TOD, and azimuth. Averages were taken over locations, as presented in table B-2.

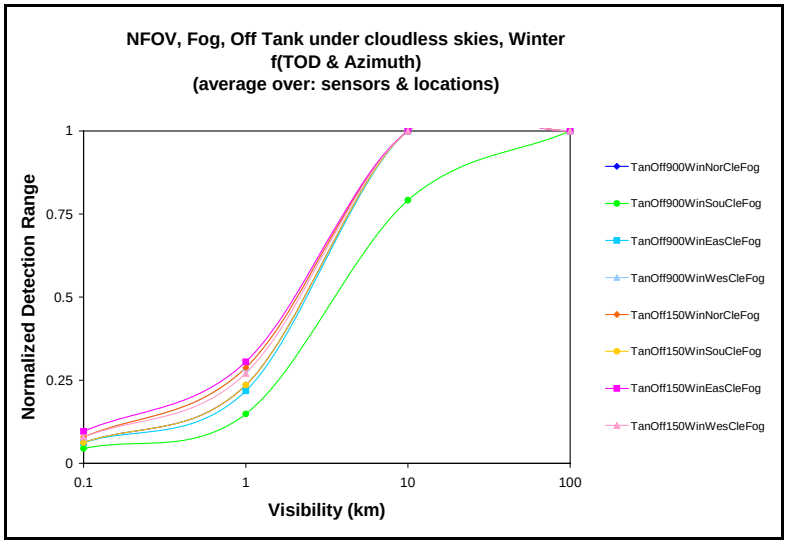

Figure B-9. Normalized detection range vs. visibility for a NFOV average sensor in a fog aerosol viewing an inactive tank under clear skies in the winter as a function of TOD and azimuth. Averages were taken over locations, as presented in table B-2.

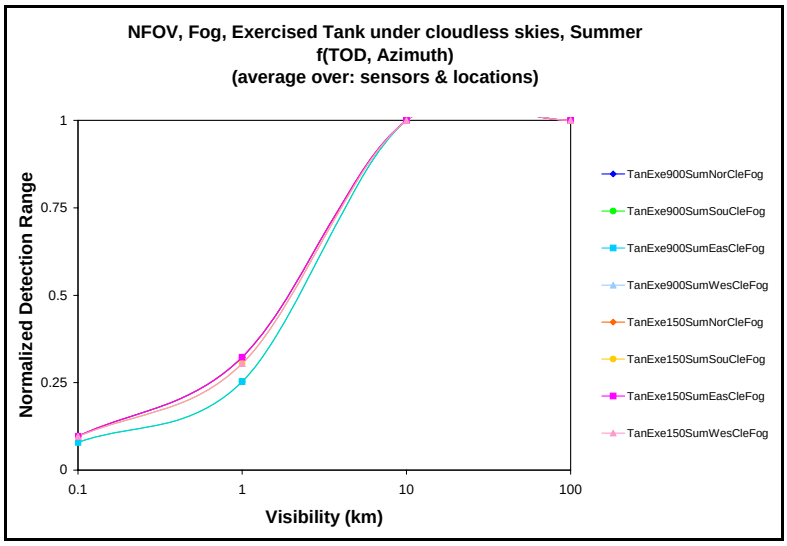

Figure B-10. Normalized detection range vs. visibility for a NFOV average sensor, in a fog aerosol, viewing an exercised tank under clear skies in the summer, as a function of TOD, and azimuth. Averages were taken over locations, as presented in table B-2.

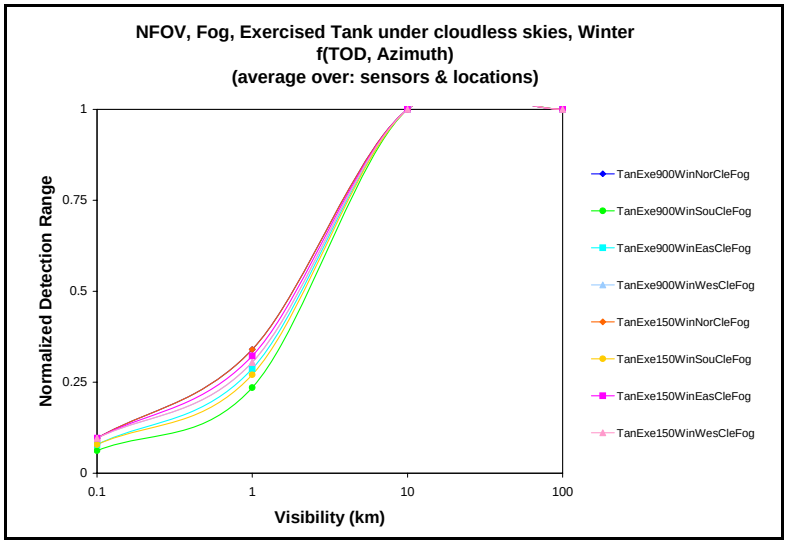

Figure B-11. Normalized detection range vs. visibility for a NFOV average sensor in a fog aerosol viewing an exercised tank under clear skies in the winter as a function of TOD and azimuth. Averages were taken over locations, as presented in table B-2.

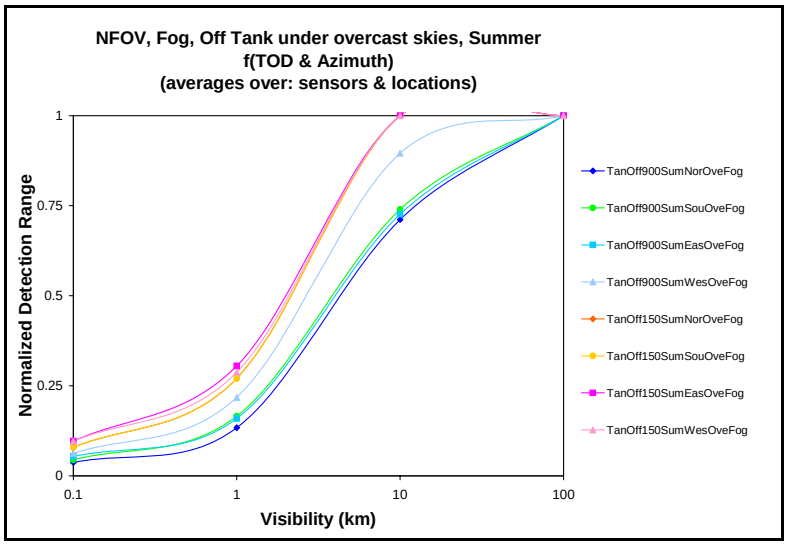

Figure B-12. Normalized detection range vs. visibility for a NFOV average sensor, in a fog aerosol, viewing an inactive tank under overcast skies in the summer, as a function of TOD, and azimuth. Averages were taken over locations, as presented in table B-2.

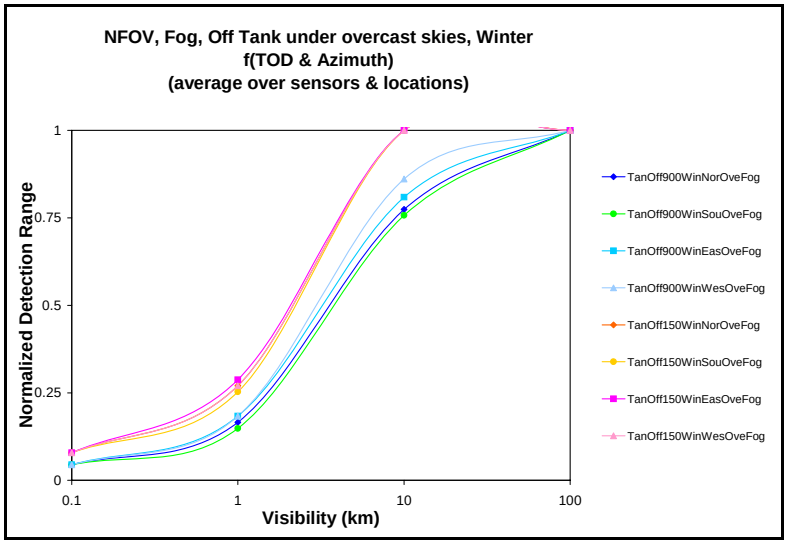

Figure B-13. Normalized detection range vs. visibility for a NFOV average sensor in a fog aerosol viewing an inactive tank under overcast skies in the winter as a function of TOD and azimuth. Averages were taken over locations, as presented in table B-2.

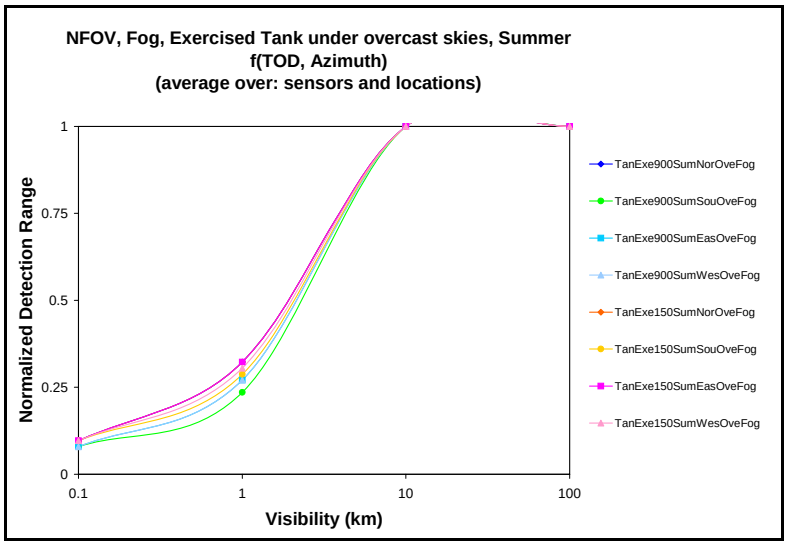

Figure B-14. Normalized detection range vs. visibility for a NFOV average sensor, in a fog aerosol, viewing an exercised tank under overcast skies in the summer, as a function of TOD, and azimuth. Averages were taken over locations, as presented in table B-2.

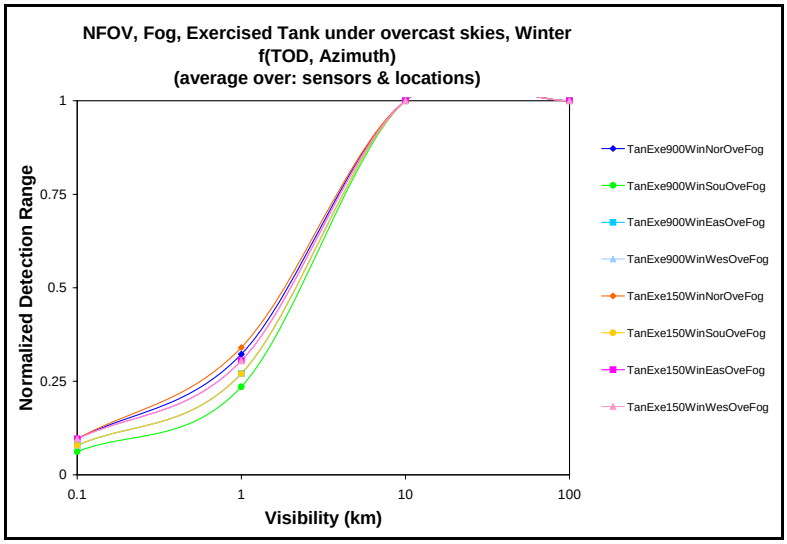

Figure B-15. Normalized detection range vs. visibility for a NFOV average sensor in a fog aerosol viewing an exercised tank under overcast skies in the winter as a function of TOD and azimuth. Averages were taken over locations, as presented in table B-2.

INTENTIONALLY LEFT BLANK.

Appendix C. Third-Order Polynomial Coefficients and their Curves for the Rural Aerosol for a NFOV and WFOV Average IR Sensor

Table C-1. Third-order polynomial coefficients curve fit to averaged quantities as represented by moniker for and average sensor viewing through a rural aerosol. WFOV results are shown.

Moniker	a0	a1	a2	a3	Average Maximum Detection Range
150CleRur	0.976	0.139	-0.168	0.052	3.60
150OveRur	0.972	0.146	-0.171	0.053	3.59
900CleRur	0.974	0.162	-0.208	0.067	3.40
900OveRur	0.849	0.249	-0.138	0.026	3.25
Tan900CleRur	1.077	0.073	-0.249	0.097	2.61
Tan150CleRur	0.989	0.099	-0.131	0.042	2.80
Tan900OveRur	0.923	0.183	-0.151	0.039	2.65
Tan150OveRur	0.988	0.103	-0.136	0.044	2.79
TanExe150OveRur	0.989	0.094	-0.123	0.039	2.81
TanExe900OveRur	0.987	0.119	-0.158	0.051	2.78
TanExe150CleRur	0.989	0.092	-0.121	0.039	2.82
TanExe900CleRur	0.988	0.114	-0.151	0.049	2.79
TanOff900CleRur	1.182	0.024	-0.364	0.153	2.40
TanOff150CleRur	0.988	0.106	-0.141	0.045	2.78
TanOff150OveRur	0.988	0.111	-0.148	0.048	2.77
TanOff900OveRur	0.857	0.249	-0.144	0.027	2.51
TanOff900SumOveRur	0.840	0.258	-0.136	0.024	2.42
TanOff900WinOveRur	0.837	0.274	-0.147	0.025	2.53
TanOff150SumOveRur	0.987	0.105	-0.139	0.045	2.77
TanOff150WinOveRur	0.989	0.131	-0.177	0.057	2.74
TanOff900NorOveRur	0.814	0.281	-0.123	0.015	2.39
TanOff900EasOveRur	0.833	0.263	-0.133	0.022	2.39
TanOff900WesOveRur	0.934	0.196	-0.181	0.050	2.67
TanOff900SouOveRur	0.843	0.260	-0.136	0.023	2.58
TanExe900SumOveRur	0.987	0.119	-0.158	0.051	2.78
TanExe900WinOveRur	0.990	0.119	-0.163	0.053	2.79
TanExe150SumOveRur	0.988	0.091	-0.118	0.038	2.81
TanExe150WinOveRur	0.991	0.101	-0.137	0.044	2.81
TanExe900NorOveRur	0.990	0.090	-0.117	0.038	2.85
TanExe900EasOveRur	0.989	0.121	-0.163	0.053	2.77
TanExe900WesOveRur	0.988	0.118	-0.159	0.051	2.78
TanExe900SouOveRur	0.982	0.147	-0.191	0.061	2.73
TanExe150NorOveRur	0.990	0.085	-0.110	0.035	2.85
TanExe150EasOveRur	0.989	0.091	-0.118	0.038	2.82
TanExe150WesOveRur	0.989	0.093	-0.123	0.039	2.81
TanExe150SouOveRur	0.988	0.107	-0.142	0.046	2.78
TanExe900NorCleRur	0.990	0.089	-0.116	0.037	2.85
TanExe900EasCleRur	0.989	0.123	-0.168	0.054	2.76
TanExe900WesCleRur	0.989	0.098	-0.129	0.041	2.82

Moniker	a0	a1	a2	a3	Average Maximum Detection Range
TanExe900SouCleRur	0.982	0.147	-0.192	0.061	2.72
TanExe150NorCleRur	0.990	0.083	-0.108	0.034	2.85
TanExe150EasCleRur	0.989	0.087	-0.113	0.036	2.83
TanExe150WesCleRur	0.989	0.094	-0.126	0.041	2.80
TanExe150SouCleRur	0.988	0.105	-0.139	0.045	2.79
TanOff900NorCleRur	1.321	-0.067	-0.466	0.210	2.48
TanOff900EasCleRur	1.608	-0.226	-0.736	0.348	1.84
TanOff900WesCleRur	0.987	0.115	-0.152	0.049	2.79
TanOff900SouCleRur	0.898	0.226	-0.178	0.045	2.43
TanOff150NorCleRur	0.988	0.108	-0.144	0.046	2.78
TanOff150EasCleRur	0.989	0.094	-0.123	0.039	2.81
TanOff150WesCleRur	0.988	0.109	-0.146	0.047	2.77
TanOff150SouCleRur	0.988	0.114	-0.152	0.049	2.77
TanOff900SumNorCleRur	0.708	0.352	-0.040	-0.031	2.62
TanOff900SumEasCleRur	0.792	0.292	-0.103	0.004	2.84
TanOff900SumWesCleRur	0.987	0.116	-0.153	0.049	2.78
TanOff900SumSouCleRur	0.915	0.211	-0.172	0.044	2.71
TanOff150SumNorCleRur	0.987	0.110	-0.147	0.048	2.76
TanOff150SumEasCleRur	0.988	0.092	-0.119	0.038	2.81
TanOff150SumWesCleRur	0.988	0.104	-0.139	0.045	2.78
TanOff150SumSouCleRur	0.987	0.102	-0.133	0.042	2.78
TanOff900WinNorCleRur	0.981	0.159	-0.207	0.066	2.74
TanOff90Win0EasCleRur	0.937	0.196	-0.188	0.053	2.70
TanOff900WinWesCleRur	0.988	0.122	-0.163	0.053	2.80
TanOff900WinSouCleRur	0.932	0.220	-0.235	0.071	2.22
TanOff150WinNorCleRur	0.988	0.107	-0.142	0.045	2.83
TanOff150WinEasCleRur	0.990	0.100	-0.134	0.043	2.81
TanOff150WinWesCleRur	0.989	0.125	-0.169	0.054	2.76
TanOff150WinSouCleRur	0.987	0.145	-0.198	0.064	2.74
TanExe900SumNorCleRur	0.990	0.091	-0.119	0.038	2.85
TanExe900SumEasCleRur	0.988	0.127	-0.173	0.056	2.75
TanExe900SumWesCleRur	0.989	0.098	-0.129	0.041	2.81
TanExe900SumSouCleRur	0.987	0.136	-0.183	0.059	2.74
TanExe150SumNorCleRur	0.988	0.086	-0.109	0.034	2.85
TanExe150SumEasCleRur	0.988	0.087	-0.111	0.035	2.83
TanExe150SumWesCleRur	0.989	0.093	-0.123	0.040	2.80
TanExe150SumSouCleRur	0.987	0.097	-0.126	0.041	2.81
TanExe900WinNorCleRur	0.995	0.082	-0.114	0.037	2.85
TanExe90Win0EasCleRur	0.991	0.117	-0.159	0.052	2.78
TanExe900WinWesCleRur	0.990	0.099	-0.134	0.043	2.85
TanExe900WinSouCleRur	0.988	0.151	-0.207	0.067	2.74
TanExe150WinNorCleRur	0.996	0.077	-0.108	0.035	2.85
TanExe150WinEasCleRur	0.991	0.089	-0.119	0.038	2.85
TanExe150WinWesCleRur	0.991	0.100	-0.136	0.044	2.81
TanExe150WinSouCleRur	0.990	0.124	-0.169	0.055	2.76
TanOff900SumNorOveRur	0.745	0.320	-0.082	-0.007	2.20
TanOff900SumEasOveRur	0.772	0.305	-0.103	0.004	2.10
TanOff900SumWesOveRur	0.963	0.173	-0.196	0.059	2.68
TanOff900SumSouOveRur	0.844	0.256	-0.144	0.027	2.62

Moniker	a0	a1	a2	a3	Average Maximum Detection Range
TanOff150SumNorOveRur	0.987	0.113	-0.150	0.049	2.75
TanOff150SumEasOveRur	0.988	0.098	-0.126	0.040	2.79
TanOff150SumWesOveRur	0.987	0.101	-0.133	0.043	2.78
TanOff150SumSouOveRur	0.987	0.109	-0.145	0.047	2.77
TanOff900WinNorOveRur	0.815	0.285	-0.142	0.023	2.47
TanOff900Win0EasOveRu	0.869	0.250	-0.168	0.038	2.56
TanOff900WinWesOveRur	0.870	0.257	-0.161	0.032	2.63
TanOff900WinSouOveRur	0.793	0.305	-0.119	0.009	2.45
TanOff150WinNorOveRur	0.989	0.129	-0.174	0.056	2.74
TanOff150WinEasOveRur	0.991	0.124	-0.169	0.055	2.74
TanOff150WinWesOveRur	0.990	0.126	-0.171	0.055	2.74
TanOff150WinSouOveRur	0.988	0.144	-0.195	0.063	2.73
TanExe900SumNorOveRur	0.990	0.091	-0.119	0.038	2.85
TanExe900SumEasOveRur	0.988	0.125	-0.169	0.055	2.77
TanExe900SumWesOveRur	0.988	0.115	-0.153	0.049	2.78
TanExe900SumSouOveRur	0.981	0.147	-0.192	0.062	2.72
TanExe150SumNorOveRur	0.988	0.087	-0.110	0.035	2.85
TanExe150SumEasOveRur	0.988	0.087	-0.111	0.035	2.81
TanExe150SumWesOveRur	0.988	0.091	-0.118	0.038	2.81
TanExe150SumSouOveRur	0.987	0.101	-0.133	0.043	2.78
TanExe900WinNorOveRur	0.994	0.084	-0.115	0.038	2.85
TanExe900WinEasOveRur	0.990	0.119	-0.163	0.053	2.78
TanExe900WinWesOveRur	0.990	0.125	-0.171	0.056	2.78
TanExe900WinSouOveRur	0.987	0.149	-0.204	0.066	2.75
TanExe150WinNorOveRur	0.994	0.082	-0.112	0.037	2.85
TanExe150WinEasOveRur	0.991	0.099	-0.133	0.043	2.81
TanExe150WinWesOveRur	0.991	0.100	-0.136	0.044	2.81
TanExe150WinSouOveRur	0.989	0.124	-0.167	0.054	2.77

Table C-2. Third-order polynomial coefficients curve fit to averaged quantities as represented by moniker for an average sensor viewing through a rural aerosol. NFOV results are shown. Coefficients in blue have associated curves presented in the graphs in this appendix.

Moniker	a0	a1	a2	a3	Average Maximum Detection Range
150CleRur	0.866	0.320	-0.248	0.061	8.88
150OveRur	0.849	0.331	-0.233	0.053	8.88
900CleRur	0.838	0.326	-0.238	0.057	8.51
900OveRur	0.645	0.424	-0.077	-0.023	8.12
Tan900CleRur	1.004	0.227	-0.370	0.128	7.42
Tan150CleRur	0.930	0.274	-0.289	0.085	7.80
Tan900OveRur	0.753	0.372	-0.158	0.017	7.50
Tan150OveRur	0.921	0.281	-0.283	0.081	7.80
TanExe150OveRur	0.947	0.263	-0.302	0.092	7.80
TanExe900OveRur	0.890	0.304	-0.264	0.070	7.80
TanExe150CleRur	0.951	0.259	-0.303	0.093	7.80
TanExe900CleRur	0.902	0.295	-0.272	0.075	7.80
TanOff900CleRur	1.127	0.145	-0.488	0.192	6.95
TanOff150CleRur	0.909	0.289	-0.274	0.076	7.80
TanOff150OveRur	0.895	0.299	-0.265	0.071	7.80
TanOff900OveRur	0.609	0.442	-0.047	-0.038	7.18
TanOff900SumOveRur	0.597	0.441	-0.042	-0.039	6.98
TanOff900WinOveRur	0.592	0.467	-0.032	-0.050	7.57
TanOff150SumOveRur	0.888	0.299	-0.254	0.066	7.80
TanOff150WinOveRur	0.908	0.301	-0.290	0.081	7.80
TanOff900NorOveRur	0.571	0.457	-0.019	-0.051	6.91
TanOff900EasOveRur	0.590	0.435	-0.038	-0.038	6.63
TanOff900WesOveRur	0.687	0.422	-0.100	-0.016	7.78
TanOff900SouOveRur	0.583	0.457	-0.026	-0.049	7.36
TanExe900SumOveRur	0.892	0.303	-0.265	0.070	7.80
TanExe900WinOveRur	0.936	0.282	-0.311	0.093	7.80
TanExe150SumOveRur	0.935	0.268	-0.288	0.085	7.80
TanExe150WinOveRur	0.979	0.250	-0.338	0.109	7.80
TanExe900NorOveRur	0.976	0.246	-0.327	0.105	7.80
TanExe900EasOveRur	0.884	0.310	-0.262	0.068	7.80
TanExe900WesOveRur	0.904	0.297	-0.277	0.076	7.80
TanExe900SouOveRur	0.797	0.364	-0.191	0.030	7.80
TanExe150NorOveRur	0.969	0.244	-0.313	0.099	7.80
TanExe150EasOveRur	0.956	0.257	-0.308	0.095	7.80
TanExe150WesOveRur	0.948	0.263	-0.302	0.092	7.80
TanExe150SouOveRur	0.915	0.287	-0.282	0.080	7.80
TanExe900NorCleRur	0.977	0.245	-0.327	0.105	7.80
TanExe900EasCleRur	0.874	0.316	-0.253	0.063	7.80
TanExe900WesCleRur	0.963	0.256	-0.319	0.100	7.80
TanExe900SouCleRur	0.795	0.363	-0.189	0.030	7.80
TanExe150NorCleRur	0.971	0.243	-0.313	0.100	7.80
TanExe150EasCleRur	0.966	0.247	-0.311	0.098	7.80
TanExe150WesCleRur	0.946	0.264	-0.301	0.091	7.80
TanExe150SouCleRur	0.923	0.282	-0.288	0.083	7.80

Moniker	a0	a1	a2	a3	Average Maximum Detection Range
TanOff900NorCleRur	1.263	0.068	-0.599	0.250	7.53
TanOff900EasCleRur	1.806	-0.269	-1.089	0.511	5.27
TanOff900WesCleRur	0.917	0.289	-0.289	0.083	7.80
TanOff900SouCleRur	0.645	0.417	-0.085	-0.018	7.03
TanOff150NorCleRur	0.899	0.296	-0.267	0.072	7.80
TanOff150EasCleRur	0.950	0.261	-0.304	0.093	7.80
TanOff150WesCleRur	0.906	0.292	-0.274	0.076	7.80
TanOff150SouCleRur	0.880	0.309	-0.252	0.064	7.80
TanOff900SumNorCleRur	0.468	0.514	0.068	-0.096	8.05
TanOff900SumEasCleRur	0.561	0.492	0.002	-0.069	8.34
TanOff900SumWesCleRur	0.914	0.291	-0.287	0.081	7.80
TanOff900SumSouCleRur	0.666	0.424	-0.090	-0.019	7.74
TanOff150SumNorCleRur	0.861	0.317	-0.232	0.054	7.80
TanOff150SumEasCleRur	0.937	0.266	-0.289	0.086	7.80
TanOff150SumWesCleRur	0.896	0.295	-0.260	0.069	7.80
TanOff150SumSouCleRur	0.900	0.293	-0.265	0.072	7.80
TanOff900WinNorCleRur	0.809	0.362	-0.208	0.037	7.80
TanOff90Win0EasCleRur	0.738	0.404	-0.147	0.006	7.80
TanOff900WinWesCleRur	0.965	0.269	-0.342	0.108	7.80
TanOff900WinSouCleRur	0.658	0.408	-0.107	-0.006	6.87
TanOff150WinNorCleRur	0.978	0.255	-0.345	0.111	7.80
TanOff150WinEasCleRur	0.987	0.247	-0.348	0.114	7.80
TanOff150WinWesCleRur	0.937	0.283	-0.314	0.094	7.80
TanOff150WinSouCleRur	0.840	0.343	-0.234	0.051	7.80
TanExe900SumNorCleRur	0.981	0.245	-0.334	0.108	7.80
TanExe900SumEasCleRur	0.848	0.331	-0.231	0.052	7.80
TanExe900SumWesCleRur	0.965	0.255	-0.322	0.101	7.80
TanExe900SumSouCleRur	0.828	0.345	-0.216	0.043	7.80
TanExe150SumNorCleRur	0.960	0.250	-0.305	0.095	7.80
TanExe150SumEasCleRur	0.954	0.252	-0.298	0.092	7.80
TanExe150SumWesCleRur	0.932	0.270	-0.286	0.084	7.80
TanExe150SumSouCleRur	0.923	0.278	-0.282	0.081	7.80
TanExe900WinNorCleRur	1.000	0.229	-0.343	0.114	7.80
TanExe90Win0EasCleRur	0.970	0.262	-0.341	0.109	7.80
TanExe900WinWesCleRur	0.993	0.241	-0.350	0.116	7.80
TanExe900WinSouCleRur	0.844	0.342	-0.240	0.054	7.80
TanExe150WinNorCleRur	1.000	0.226	-0.340	0.113	7.80
TanExe150WinEasCleRur	0.997	0.234	-0.346	0.115	7.80
TanExe150WinWesCleRur	0.987	0.244	-0.344	0.113	7.80
TanExe150WinSouCleRur	0.933	0.286	-0.313	0.093	7.80
TanOff900SumNorOveRur	0.529	0.459	0.005	-0.058	6.87
TanOff900SumEasOveRur	0.531	0.444	0.000	-0.052	5.73
TanOff900SumWesOveRur	0.717	0.412	-0.123	-0.006	7.80
TanOff900SumSouOveRur	0.578	0.458	-0.026	-0.049	7.38
TanOff150SumNorOveRur	0.860	0.317	-0.230	0.053	7.80
TanOff150SumEasOveRur	0.924	0.277	-0.282	0.081	7.80
TanOff150SumWesOveRur	0.901	0.292	-0.265	0.072	7.80
TanOff150SumSouOveRur	0.869	0.312	-0.238	0.058	7.80
TanOff900WinNorOveRur	0.569	0.488	-0.006	-0.065	7.53

Moniker	a0	a1	a2	a3	Average Maximum Detection Range
TanOff900Win0EasOveRu	0.617	0.449	-0.056	-0.036	7.52
TanOff900WinWesOveRur	0.634	0.436	-0.070	-0.028	7.72
TanOff900WinSouOveRur	0.544	0.498	0.008	-0.071	7.49
TanOff150WinNorOveRur	0.903	0.304	-0.285	0.079	7.80
TanOff150WinEasOveRur	0.943	0.279	-0.319	0.097	7.80
TanOff150WinWesOveRur	0.932	0.286	-0.309	0.092	7.80
TanOff150WinSouOveRur	0.853	0.335	-0.246	0.058	7.80
TanExe900SumNorOveRur	0.981	0.243	-0.333	0.108	7.80
TanExe900SumEasOveRur	0.875	0.315	-0.255	0.064	7.80
TanExe900SumWesOveRur	0.915	0.290	-0.287	0.081	7.80
TanExe900SumSouOveRur	0.794	0.365	-0.187	0.028	7.80
TanExe150SumNorOveRur	0.958	0.251	-0.303	0.094	7.80
TanExe150SumEasOveRur	0.945	0.261	-0.296	0.089	7.80
TanExe150SumWesOveRur	0.935	0.269	-0.289	0.086	7.80
TanExe150SumSouOveRur	0.900	0.293	-0.265	0.072	7.80
TanExe900WinNorOveRur	0.999	0.231	-0.345	0.115	7.80
TanExe900WinEasOveRur	0.954	0.276	-0.333	0.103	7.80
TanExe900WinWesOveRur	0.945	0.280	-0.324	0.099	7.80
TanExe900WinSouOveRur	0.845	0.341	-0.241	0.055	7.80
TanExe150WinNorOveRur	0.999	0.229	-0.341	0.114	7.80
TanExe150WinEasOveRur	0.988	0.243	-0.345	0.113	7.80
TanExe150WinWesOveRur	0.985	0.246	-0.344	0.112	7.80
TanExe150WinSouOveRur	0.944	0.280	-0.322	0.098	7.80

The coefficients displayed in blue in table C-2 have associated curves that are presented in the following graphs labeled figures C-1 through C-15.

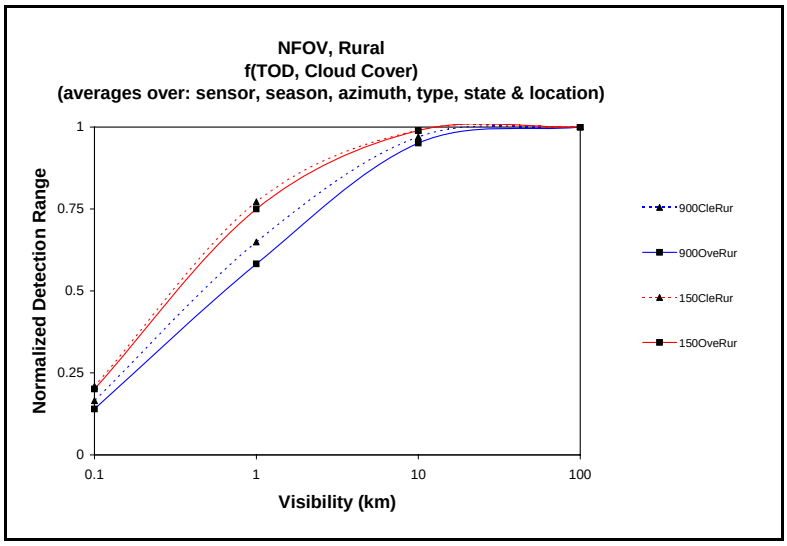

Figure C-1. Normalized detection range vs. visibility for a NFOV average sensor in a rural aerosol as a function of TOD and cloud cover. Averages were taken over seasons, locations, azimuths, target types and operating states, as presented in table C-2.

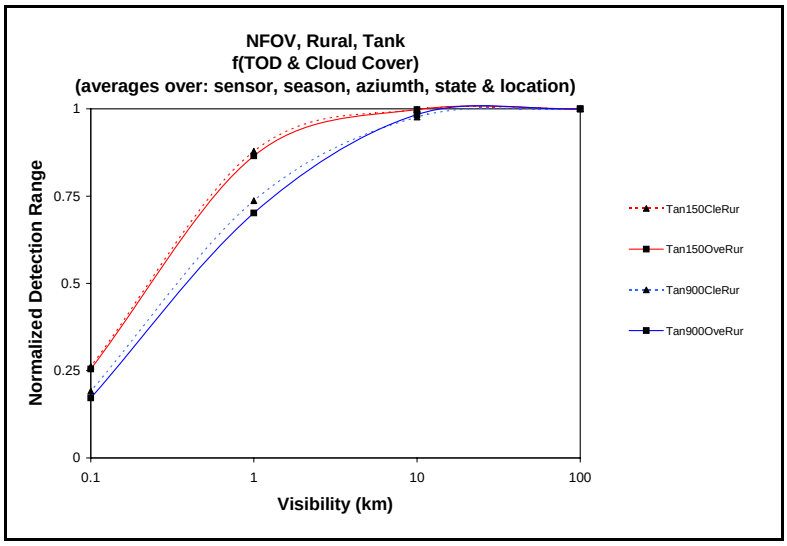

Figure C-2. Normalized detection range vs. visibility for a NFOV average sensor, in a rural aerosol, viewing a tank, as a function of time of day and cloud cover. Averages were taken over seasons, locations, azimuths, and target operating states, as presented in table C-2.

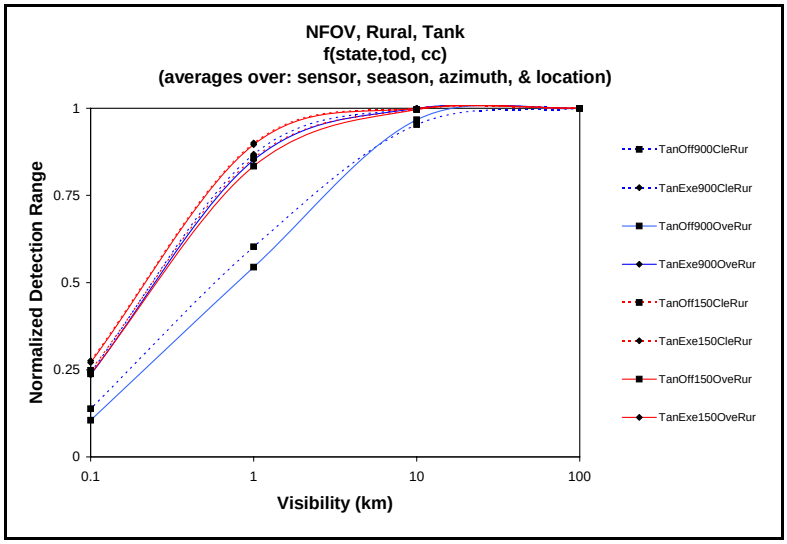

Figure C-3. Normalized detection range vs. visibility for a NFOV average sensor in a rural aerosol as a function of target operating state, time of day and cloud cover. Averages were taken over seasons, locations, and azimuths, as presented in table C-2.

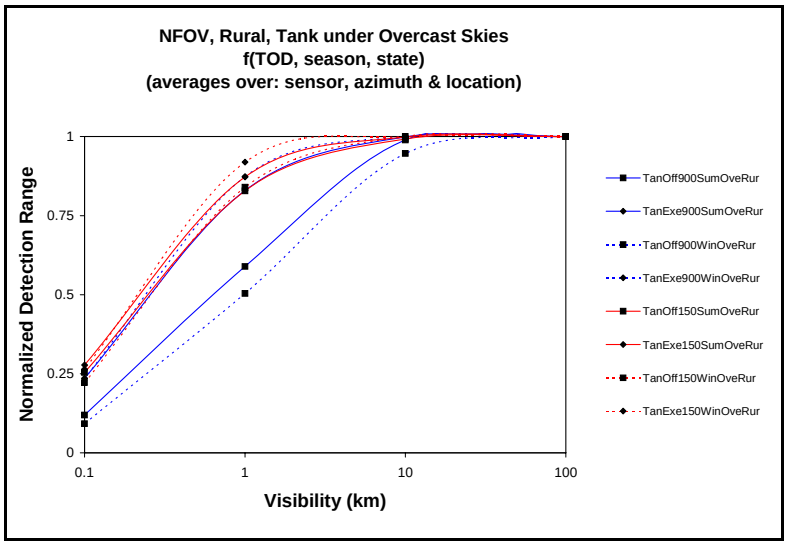

Figure C-4. Normalized detection range vs. visibility for a NFOV average sensor, in a rural aerosol, viewing a tank under overcast skies, as a function of TOD, season, and operating state. Averages were taken over locations, and azimuths, as presented in table C-2.

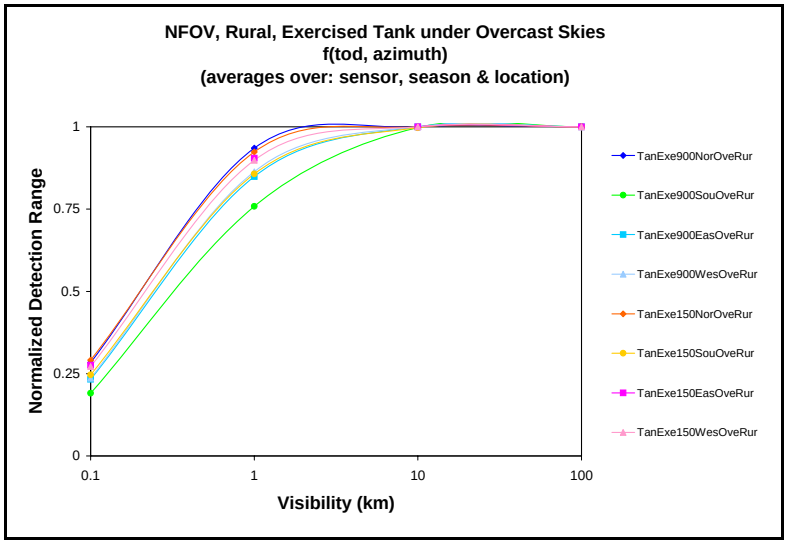

Figure C-5. Normalized detection range vs. visibility for a NFOV average sensor in a rural aerosol viewing an exercised tank under overcast skies as a function of TOD and azimuth. Averages were taken over seasons and locations, as presented in table C-2.

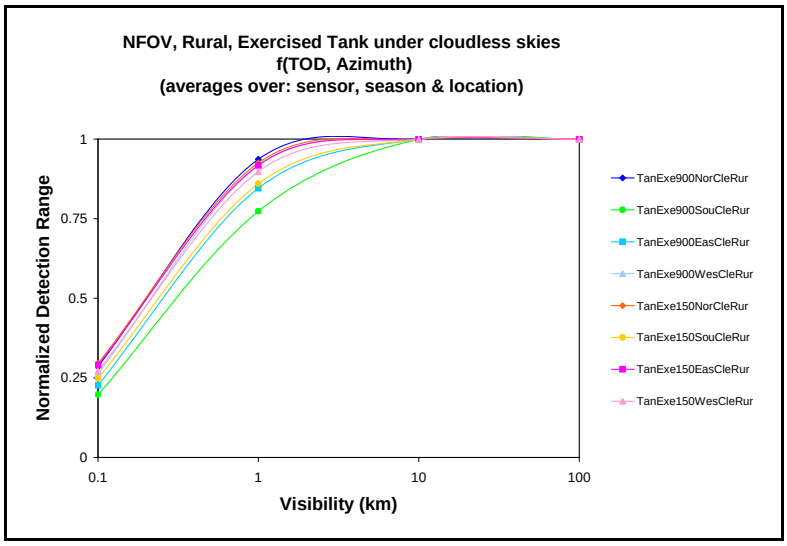

Figure C-6. Normalized detection range vs. visibility for a NFOV average sensor, in a rural aerosol, viewing an exercised tank under clear skies, as a function of TOD, and azimuth. Averages were taken over seasons and locations, as presented in table C-2.

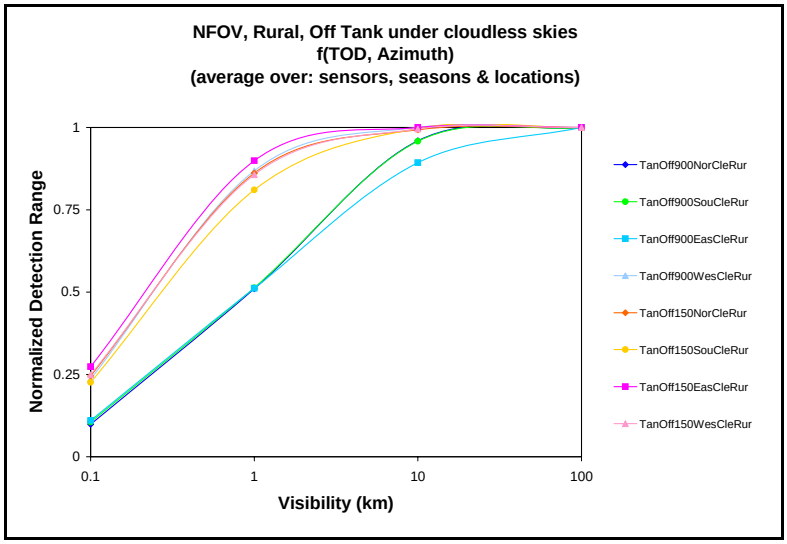

Figure C-7. Normalized detection range vs. visibility for a NFOV average sensor in a rural aerosol viewing an inactive tank under clear skies as a function of TOD and azimuth. Averages were taken over seasons and locations, as presented in table C-2.

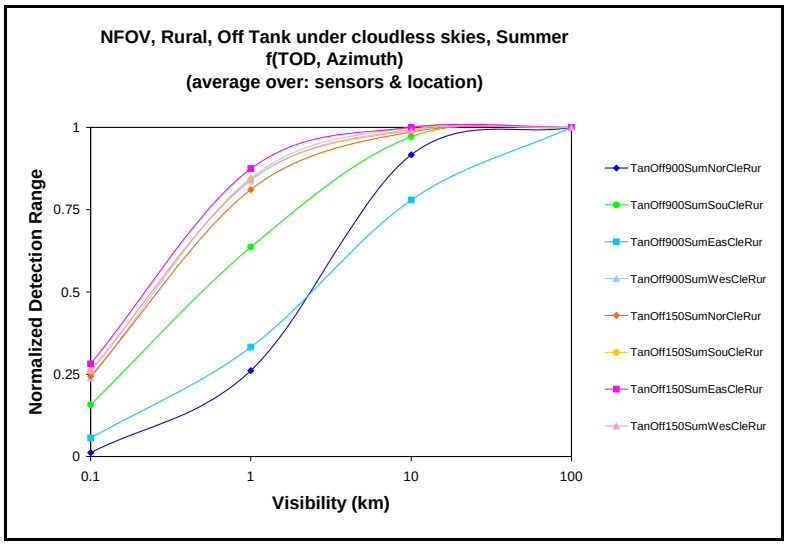

Figure C-8. Normalized detection range vs. visibility for a NFOV average sensor, in a rural aerosol, viewing an inactive tank under clear skies in the summer, as a function of TOD, and azimuth. Averages were taken over locations, as presented in table C-2.

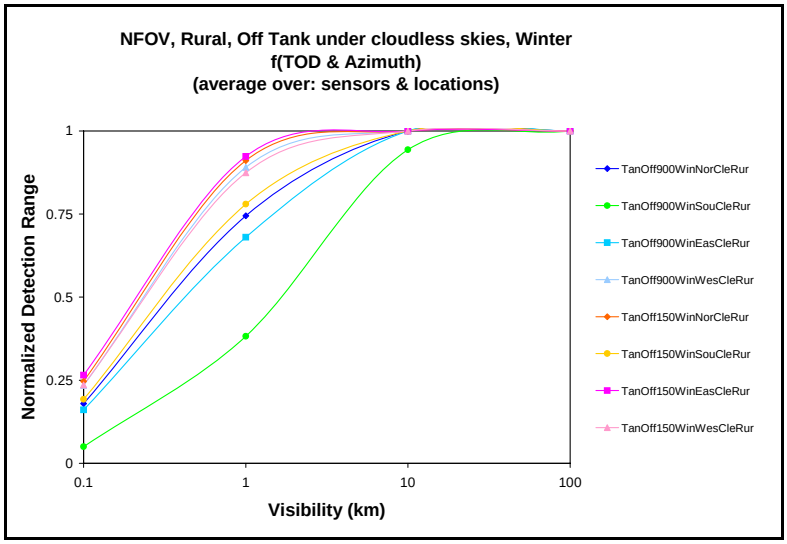

Figure C-9. Normalized detection range vs. visibility for a NFOV average sensor in a rural aerosol viewing an inactive tank under clear skies in the winter as a function of TOD and azimuth. Averages were taken over locations, as presented in table C-2.

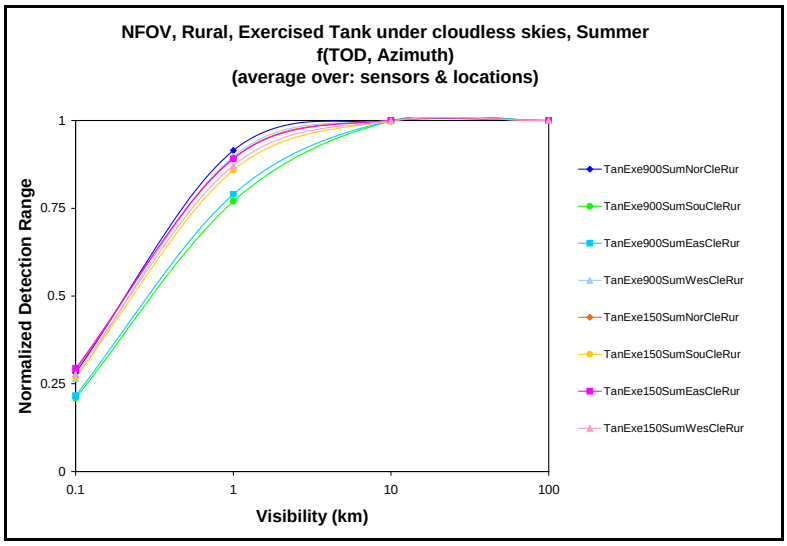

Figure C-10. Normalized detection range vs. visibility for a NFOV average sensor, in a rural aerosol, viewing an exercised tank under clear skies in the summer, as a function of TOD, and azimuth. Averages were taken over locations, as presented in table C-2.

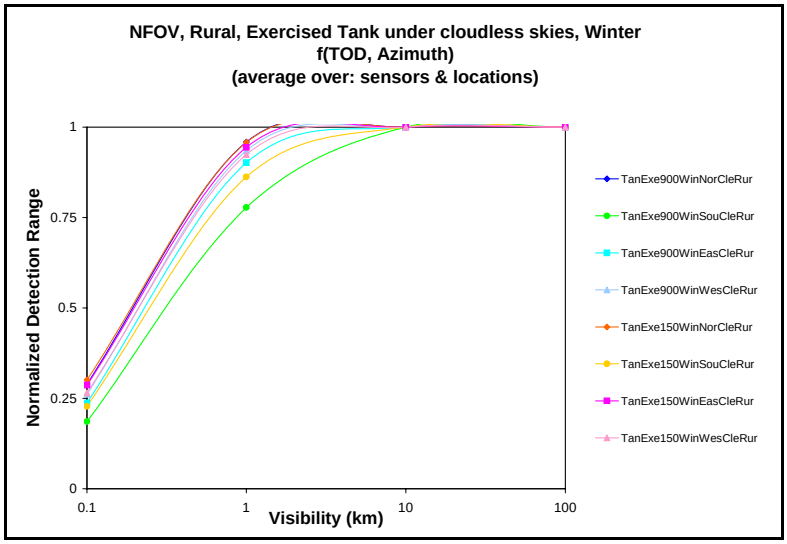

Figure C-11. Normalized detection range vs. visibility for a NFOV average sensor in a rural aerosol viewing an exercised tank under clear skies in the winter as a function of TOD and azimuth. Averages were taken over locations, as presented in table c-2.

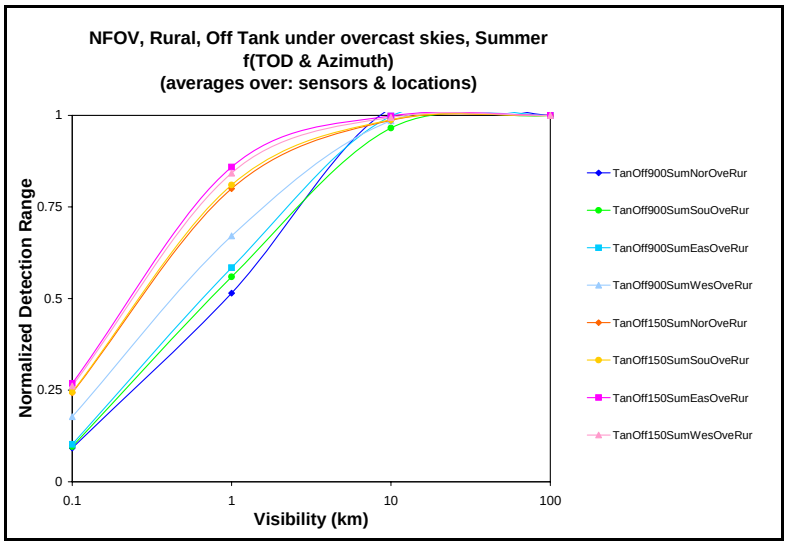

Figure C-12. Normalized detection range vs. visibility for a NFOV average sensor, in a rural aerosol, viewing an inactive tank under overcast skies in the summer, as a function of TOD, and azimuth. Averages were taken over locations, as presented in table C-2.

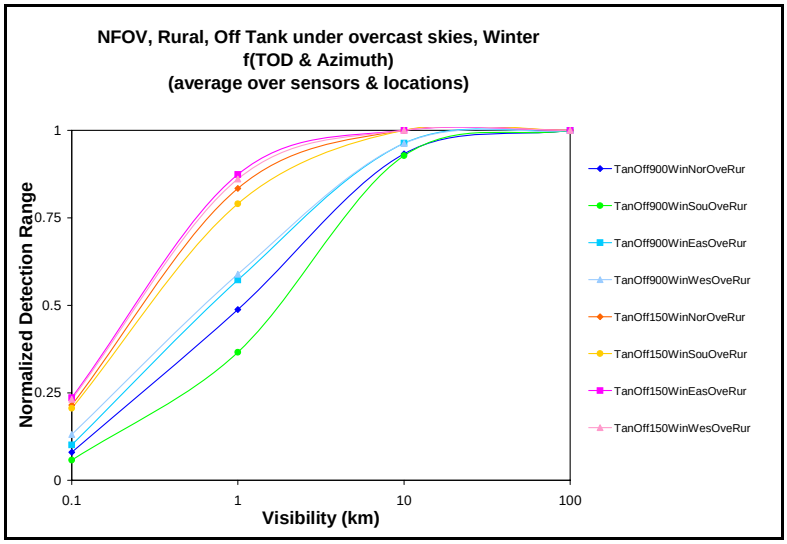

Figure C-13. Normalized detection range vs. visibility for a NFOV average sensor in a rural aerosol viewing an inactive tank under overcast skies in the winter as a function of TOD and azimuth. Averages were taken over locations, as presented in table C-2.

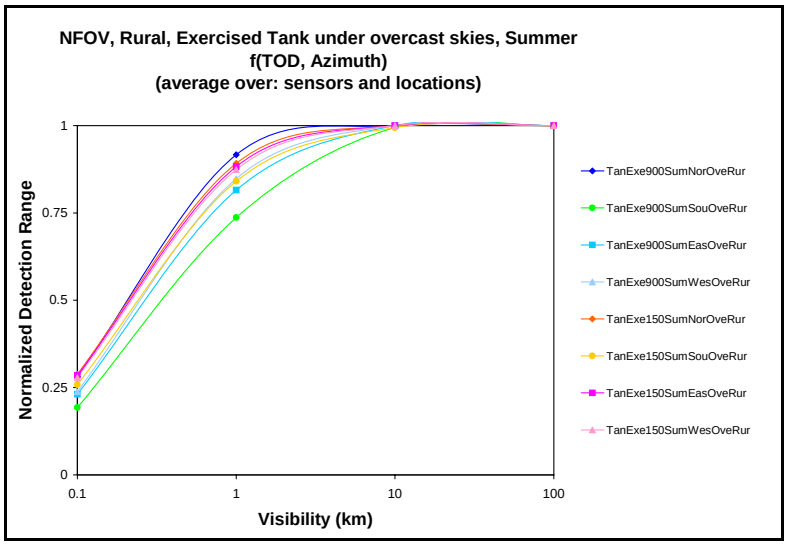

Figure C-14. Normalized detection range vs. visibility for a NFOV average sensor, in a rural aerosol, viewing an exercised tank under overcast skies in the summer, as a function of TOD, and azimuth. Averages were taken over locations, as presented in table C-2.

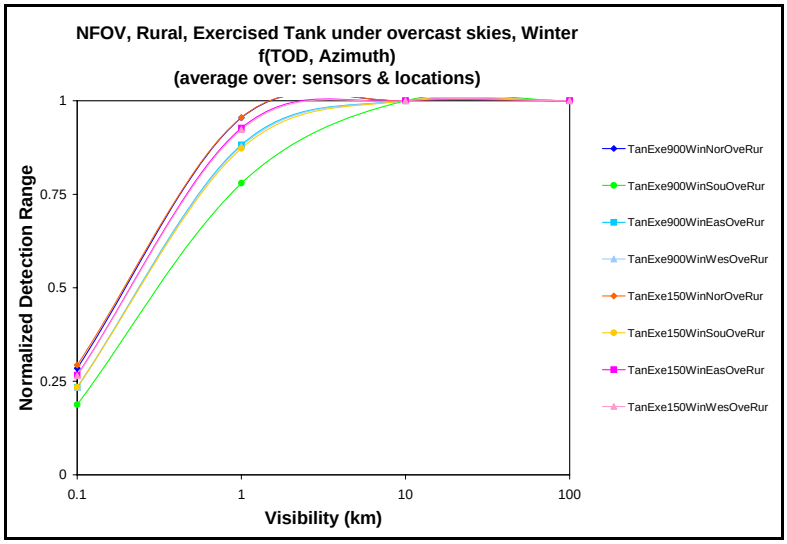

Figure C-15. Normalized detection range vs. visibility for a NFOV average sensor in a rural aerosol viewing an exercised tank under overcast skies in the winter as a function of TOD and azimuth. Averages were taken over locations, as presented in table C-2.

Abbreviations and Symbols

APC	armored personnel carrier
ARL/BED	Army Research Laboratory/Battlefield Environment Division
AWARS	Advanced Warfighting Simulation
C2	Command and Control
CASTFOREM	Combined Arms Support Task Force Evaluation Model
CBS	Corps Battle Simulation
CEM	Concepts Evaluation Model
COMBAT XXI	Combined Arms Analysis Tool for the XXIst Century
DF	direct fire
FOV	field of view
FWA	fixed-wing aircraft
HEAT	High Explosive Anti-Tank
helo	helicopter
HF	High Frequency
IR	Infrared
ISR	Intelligence Surveillance and Reconnaissance
IWEDA	Integrated Weather Effects Decision Aid
JCATS	Joint Conflict and Tactical Simulation
JSIMS	Joint Simulation System
JWARS	Joint Warfare System
LOS	Line of Sight
LWIR	long-wave IR
NFOV	narrow field of view
NVESD	Night Vision and Electronic Sensors Directorate

OneSAF	One Semi-automated Forces
OR	operations research
TACWAR	Tactical Warfare Model
TAWS	Target Acquisition Weapons Software
TAWS	Target Acquisition Weapons Software
TOD	Time of Day
TOD	time of day
TRAC	TRADOC Analysis Center
VIC	Vector in Commander
WARSIM	Warfighter's Simulation
WFOV	Wide Field of View
WFOV	wide field of vision

Distribution List

Army Research Laboratory 1
Attn: AMSRD-ARL-CI (Dr. Gowens)
Adelphi MD 20783-1197

Army Research Laboratory 1
Attn: AMSRD-ARL-CI (P. Clark)
Adelphi MD 20783-1197

Army Research Laboratory 1
Attn: AMSRD-ARL-CI (Dr. Ingram)
Adelphi MD 20783-1197

Army Research Laboratory 1
Attn: AMSRD-ARL-CI-EE (Dr. Hoock)
WSMR NM 88002-5501

Army Research Laboratory 2
Attn: AMSRD-ARL-CI-EE (Dr. Shirkey)
WSMR NM 88002-5501

Army Research Laboratory 2
Attn: AMSRD-ARL-CI-EE (Dr. O'Brien)
WSMR NM 88002-5501

Director, USA TRADOC Analysis Center 1
Attn: ATRC-WEC (D. Durda)
WSMR, NM 88002-5502

Army Research Laboratory 1
Attn: AMSRD-ARL-RO-EN (Dr. Bach)
PO Box 12211
Research Triangle Park, NC 27009

Army Materiel Systems Analysis Activity 1
Attn: AMXSY-SC (J. Mazz)
392 Hopkins Road
APG MD 21005-5071

Army Materiel Systems Analysis Activity 1
ATTN: AMSXY
APG MD 21005-5071

Army Dugway Proving Ground 1
STEDP MT M
Attn: J. Bowers
Dugway UT 84022-5000

USACE Engineer Research &
Development Center 1
Cold Regions Research and Engineering Laboratory
Attn: Dr. Koenig
72 Lyme Road, Hanover, New Hampshire, USA
03755-1290

Director, USA TRADOC Analysis Center 1
Attn: ATRC-W (P. Blechinger)
WSMR, NM 88002-5502

Director, USA TRADOC Analysis Center 1
Attn: ATRC-WA (L. Southard)
WSMR, NM 88002-5502

Director, USA TRADOC Analysis Center 1
Attn: ATRC-WEA (D. Mackey)
WSMR, NM 88002-5502

Director, USA TRAC Anal Ctr 1
Attn: ATRC-FM (T. Bailey)
255 Sedgwick Ave
Ft Leavenworth, KS 66027-2345

Director, USA TRAC Anal Ctr 1
Attn: ATRC-FMA (T. Gach)
255 Sedgwick Ave
Fort Leavenworth KS 66027-2345

Director, USA TRAC Anal Ctr 1
Attn: ATRC-FMA (S. Glasgow)
255 Sedgwick Ave
Ft Leavenworth, KS 66027-2345

United States Military Academy 1
Attn: Combat Simulation Laboratory (Dr. P. West)
West Point, NY 10996

Battle Command Simulation and Experimentation
Directorate 1
Army Model and Simulation Division
Attn: DA G37 (DAMO-SBM)
400 Army Pentagon
Washington, DC 20310-0450

USA PEO STRI 1
Attn: J. Blake
12350 Research Pkwy
Orlando, FL 32826-3276

HQ USAFA/DFLIB 1
2354 Fairchild Drive, Suite 3A10
USAF Academy, CO 80840-6214

AFMC DOW 1
Wright Patterson AFB OH 45433-5000

HQ AFWA/DNX 1
106 Peacekeeper Dr STE 2N3
Offutt AFB NE 68113-4039

Naval Research Laboratory 1
Attn: Dr. Goroch
Marine Meteorology Division, Code 7543
7 Grace Hopper Ave
Monterey, CA 93943-5006

U.S. Naval War College 1
Attn: War Gaming Department (Code 33)
686 Cushing Road
Newport, Rhode Island 02841-1207

Naval Weapons Surface Ctr 1
Attn: CODE G63
Dahlgren VA 22448-5000

JWARS 1
Attn: C. Burdick
1555 Wilson Boulevard, Suite 619
Arlington, VA 22209

Northrop Grumman Information Technology 1
Attn: Melanie Gouveia
100 Brickstone Square
Andover, MA 01810-5000

Anteon Corp. 1
Attn: Mike Adams
46 Growing Rd
Hudson, NH 03051

Northrop Grumman Corporation 1
Attn: R. Smith
E-10A BDT SEIT M&S IPT Lead
MS B06-222
2000 NASA Blvd
Melbourne, Florida 32907

AFRL/IFOIL 1
525 Brooks Rd
Rome NY 13441-4505

Tech Connect 1
AFRL/XPTC
Bldg 16, Rm 107
2275 D Street
WPAFB OH 45433-7226

WSMR Technical Library 1
Attn: STEWS IM IT
WSMR NM 88002

Technical Reports Boulder Laboratories Library 1
Attn: MC 5
325 Broadway
Boulder, CO 80305

Ruth H. Hooker Research Library 1
4555 Overlook Ave, SW
Washington, DC 20375

U.S. Army Research Laboratory 1
Attn: IMNE ALC IMS
Mail & Records Mgmt
Adelphi, MD 20783-1197

Admnstr 1
Defns Techl Info Ctr
Attn: DTIC OCP (V Maddox)
8725 John J Kingman Rd., Ste. 0944
Ft Belvoir, VA 22060-6218

U.S. Army Research Laboratory 2
Attn: AMSRD ARL CI OK TL Techl Lib
2800 Powder Mill Rd.
Adelphi, MD 20783-1197

U.S. Army Research Laboratory 2
Attn: AMSRD ARL CI OK TP Techl Lib
APG, MD 21005

Total 44

INTENTIONALLY LEFT BLANK.